JULY 2023 M.Sc. in Materials Science and Engineering İBRAHİM ARSLAN

REPUBLIC OF TÜRKİYE

GAZİANTEP UNIVERSITY

GRADUATE SCHOOL OF NATURAL & APPLIED SCIENCES

INVESTIGATION OF MICROSTRUCTURAL AND MECHANICAL PROPERTIES OF HIGH MANGANESE STEELS MANUFACTURED BY CASTING METHOD

M.Sc. THESIS

IN

MATERIALS SCIENCE AND ENGINEERING

BY

İBRAHİM ARSLAN

JULY 2023

INVESTIGATION OF MICROSTRUCTURAL AND MECHANICAL PROPERTIES OF HIGH MANGANESE STEELS MANUFACTURED BY CASTING METHOD

M.Sc. Thesis

in

Materials Science and Engineering

Gaziantep University

Supervisor

Assoc. Prof. Dr. Halil İbrahim KURT

Co-Supervisor

Assoc. Prof. Dr. Mustafa Güven GÖK

by

İbrahim ARSLAN

July 2023

I hereby declare that all information in this document has been obtained and presented in accordance with academic rules and ethical conduct. I also declare that, as required by these rules and conduct, I have fully cited and referenced all material and results that are not original to this work.

İbrahim ARSLAN

ABSTRACT

INVESTIGATION OF MICROSTRUCTURAL AND MECHANICAL PROPERTIES OF HIGH MANGANESE STEELS MANUFACTURED BY CASTING METHOD

ARSLAN, İbrahim
M.Sc. in Materials Science and Engineering
Supervisor: Assoc. Prof. Dr. Halil İbrahim KURT
Co-Supervisor: Assoc. Prof. Dr. Mustafa Güven GÖK
July 2023
74 pages

High wear-resistant castings are generally manufactured in foundries and this process requires a complex engineering knowledge. Special processes are used in the production of high wear-resistant materials, which significantly increase the wear resistance of the materials. High manganese steels are also a group of materials with high wear resistance that are produced using these processes and high engineering expertise. The cast high manganese steel parts have very high impact and wear resistance. With the advancement of technology, the need for materials with even higher impact and wear resistance is increasing day by day. The high manganese steels (GX120Mn12) produced by the casting method, also known as Hadfield steels, have a short service life as they deteriorate, melt, crack, and break on their surfaces when exposed to long periods of impact and high temperatures. Products that have expired must be replaced. This process (regular maintenance and part replacement) causes time loss and excessive cost for businesses.

In this study, ten different samples will be produced using a different process with the sand casting method. Therefore, in accordance with the purpose of this study; A kind of composite material was produced by adding master alloy “Al5Ti1B” to manganese steel materials produced by sand mold casting method, thereby improving wear resistance.Spectral analysis, Vickers hardness testing and analysis, and wear value analysis will be performed on each sample. In addition, changes in the material's internal structure will be examined using metal microscopy and Scanning Electron Microscopy (SEM). In the microstructure, it was observed that the main phase consisted of the austenite phase and the pearlite phase. It was determined that carbide compounds precipitated on the grain boundaries were formed. With the addition of Al5Ti1B, different results were obtained in hardness values, the maximum hardness was obtained as 272.56, and it was observed that the wear resistance of the materials improved.

Keywords: Casting, Manganese Steel, Super Alloy, Altibor, Al5Ti1B

ÖZET

DÖKÜM YÖNTEMİ İLE ÜRETİLEN YÜKSEK MANGANLI ÇELİKLERİN MİKRO YAPI VE MEKANİK ÖZELLİKLERİNİN İNCELENMESİ

ARSLAN, İbrahim
Yüksek Lisans Tezi, Malzeme Bilimi Ve Mühendisliği
Danışman: Doç. Dr. Halil İbrahim KURT
İkinci Danışman: Dr. Öğr. Üyesi Mustafa Güven GÖK
Temmuz 2023
74 sayfa

Dökümhanelerde genellikle aşınma direnci yüksek döküm parçalarının imalatı yapılmak istenmektedir. Bu işlem oldukça karmaşık ve iyi bir mühendislik bilgisi gerektirmektedir. Aşınma direnci yüksek malzemelerin üretiminde özel bazı proseslerden yararlanılmaktadır. Bu prosesler sonucunda malzemelerin aşınma dirençleri oldukça artmaktadır. Yüksek Mangan Çelikleri de bu prosesler ve yüksek mühendislik gerektiren işlemlerden sonra ortaya çıkan yüksek aşınma direncine sahip malzeme grubudur. Dökümü yapılmakta olan yüksek mangan çelik, parçalarının oldukça yüksek darbe ve aşınma direnci bulunmaktadır. Gelişmekte olan teknolojiyle beraber darbe ve aşınma direnci daha yüksek malzemelere ihtiyaç her geçen gün daha da artmaktadır. Döküm yöntemiyle üretilmekte olan ve Hadfield Çeliği olarak da bilinen yüksek manganlı çelikler (GX120Mn12), uzun süre darbeye ve yüksek ısıya maruz kaldıklarında; yüzeylerinde bozulma, erime, çatlama ve kırılmalar meydana gelerek; kısa bir servis süresinden sonra kullanım ömürleri dolmaktadır. Ömürleri dolan ürünlerin değiştirilmesi gerekmektedir. Bu işlem de (düzenli bakım ve parça değişimi) işletmeler için zaman kaybına ve aşırı maliyete sebep olmaktadır.

Bu çalışmada farklı bir proses kullanılarak kum kalıba döküm yöntemi ile 10 farklı numune üretilecektir. Dolayısı ile bu çalışmanın amacı; kum kalıba döküm yöntemi ile üretilen manganlı çelik malzemelere, master alaşımı olan “Al5Ti1B” ilave ederek bir tür kompozit malzeme üretmek ve bu sayede aşınma direncini iyileştirmektir. Bu numunelerin her birine spektral analiz, Vickers sertlik test ve analizleri, aşınma değerleri incelenmiştir. Ayrıca metal mikroskobu ve Taramalı Elektron Mikroskobu (SEM) ile malzemenin içyapısındaki değişimler incelenmiştir. Mikroyapıda ana fazın östenit fazı ile birlikte perlit fazından oluştuğu görülmüştür. Tane sınırlarına çökelen karbür bileşiklerinin meydana geldiği tespit edilmiştir. Al5Ti1B ilavesi ile sertlik değerlerinde farklı sonuçlar elde edilmiş olup maksimum” sertlik 272.56 olarak ölçülmüştür. Buna istinaden malzemelerin aşınma dayanımının geliştiği görülmüştür.

Anahtar Kelimeler: Döküm, Manganlı Çelik, Süper Alaşım, Altibor, Al5Ti1B

''Dedicated to my family''

ACKNOWLEDGEMENTS

I would like to thank my supervisor, Assoc. Prof. Dr. Halil İbrahim KURT and Assoc. Prof. Dr. Mustafa Güven GÖK for them guidance and support throughout the study. I am thankful for them encouragement and motivation.

I would like to express my love and gratitude to my family and to my colleagues for their support, always best wishes.

This work is supported by Gaziantep University BAP through Project MF.YLT.22.02

TABLE OF CONTENTS

Page

LIST OF FIGURES

Page

LIST OF TABLES

Page

LIST OF SYMBOLS

Al5Ti1B	: Altibor (Master Alloy)
C	: Carbon
Al	: Aluminum
Cr	: Chromium
Mn	: Manganese
P	: Phosphorus
Mo	: Molybdenum
Ni	: Nickel
S	: Sulfur
Si	: Silicon
V	: Vanadium
Mg	: Magnesium
Fe	: Iron
HNO_3	: Nitric Acid
HB	: Hardness Brinell
HV	: Hardness Vickers
Fe-C	: Iron-Carbon
°C	: Degrees Celsius

LIST OF ABBREVIATIONS

AISI	: American Iron and Steel Institute
ASTM	: American Society for Testing and Materials
BCC	: Body-centered cubic
CNC	: Computer Numerical Control
EDS	: Energy Dispersive X-ray Analysis
FCC	: Face-centered cubic
Fe_3C	: Iron/Carbon Alloy Phase Diagram
HCP	: Hexagonal Close-packed
HMS	: High Manganese Steels
ISO	: International Organization for Standardization
MPA	: Mega Pascal
SEM	: Scanning Electron Microscope
SFE	: Stacking Fault Energy
TRIP	: Transformation Induced Plasticity
TWIP	: Transformation Induced Plasticity
XRD	: X-ray Diffraction

CHAPTER 1
INTRODUCTION

1.1 General Introduction

According to their intended use in construction, grinding, mining, etc. sectors, most of the aggregates are obtained from quarries by mechanical processes. These mechanical operations are carried out in machines called crushers. Large blocks of rock, hard mines, etc. are thrown into these crushers and reduced in certain proportions and sized with the help of sieves according to the area to be used. There is casting materials used as consumables in the crusher. Depending on the hardness and abrasiveness of the shredded material, this casting material sometimes wears out in a very short time and becomes unusable. Premature wear of the casting parts exposed to wear under high loads not only reduces the service life of the parts, but also increases the production costs and the repair costs of the machine platforms significantly. Such specific parts should be selected from wear-resistant materials whose material selections are suitable for working conditions [1].

Hardness is the most important factor affecting the wear resistance of materials. In general, as the hardness of the materials increases and the amount of wear decreases in the same direction. A significant increase in hardness can be achieved by increasing the carbon content in the structure as much as possible and by adding other alloying elements. On the other hand, since the microstructures of different materials with the same hardness are different, the amount of wear also differs. Therefore, the second important factor for obtaining optimum properties is the microstructure of the material. Therefore, it can be stated that the best method to improve the wear properties of materials is to optimize the material, hardness and microstructure that are compatible with the operating conditions. This can be achieved by conducting experiments in the most suitable conditions for the real working environments of various types of materials, mostly with different hardness and microstructure, in order to minimize the research and development costs as much as possible.

High manganese steels, with their excellent hardness-ductility combination, make it possible to produce parts with high strength, high toughness and high wear resistance. However, the primary reason to choose austenitic manganese steels for any particular application is that they are materials with high toughness rather than wear resistance. Because when these steels are subjected to impact loads, they harden considerably while exhibiting superior toughness properties. However, due to their low yield strength, large deformations can occur under high loads and cause parts to break before work hardening begins. This is particularly common in the mining industry in the impact and wear-resistant moving pallet systems of construction equipment. Because these parts harden with the load applied by the rollers walking on them and they undergo plastic deformation due to the pushing and pulling forces they apply to each other. Therefore, optimization of important mechanical properties of high manganese steels such as ultimate yield strength, tensile strength, and wear resistance is the key factor for extending material service life in critical engineering applications.

In this study, it is aimed to improve the microstructure and mechanical properties of high manganese steels, which are widely used in the sectors, mining, construction, cement, etc. by adding Al5Ti1B at certain rates. [2].

1.2 General Properties, Alloys and Usage Areas of High Manganese Steels

1.2.1. General Properties of High Manganese Steels (Hadfield Steels)

Steels that contain 1-1.4% carbon and 10-20% high manganese in industrial applications and whose structure can remain 100% austenitic under suitable cooling conditions are called austenitic manganese steel. These steels are also known as Hadfield steel, as they were first patented by Sir Robert Hadfield in England in 1883 [2,3].

Before the discovery of high manganese steels, the strength values and ductility of the materials were inversely proportional to each other. This is because strength and ductility are inversely proportional. As the ductility of the material increases, its strength decreases, and as the strength increases, its ductility decreases [2,4]. The situation is very different for the high manganese steels discovered by Sir Robert Hadfield. In high manganese steels, the ductility and strength of the material are in perfect harmony. Compared to the tempered steels, in strength, these steels are as good as they are, while their formability properties are at least ten times better. Figure 1 shows the comparison of the elongation and strength values of different material groups [2, 5-7].

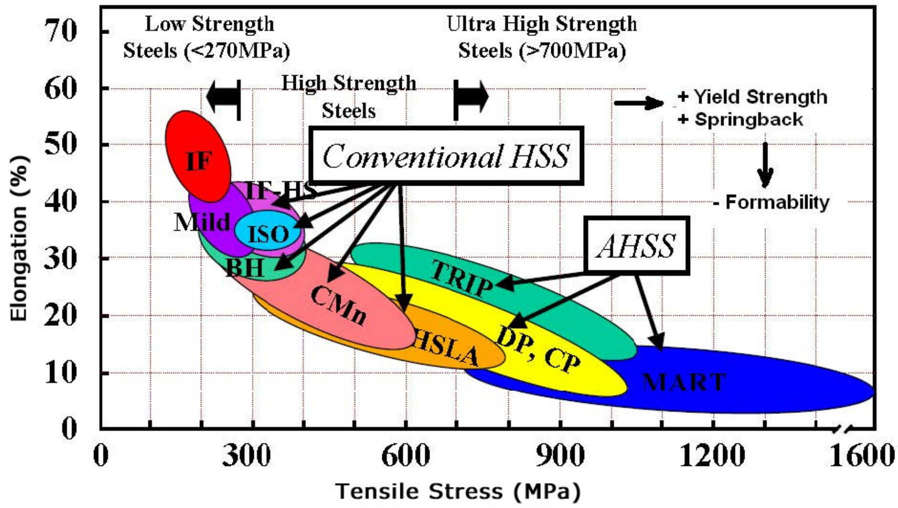

Figure 1: Comparison of strength and elongation values of different steel grades [2, 5]

High Manganese Steels have a brittle structure due to carbide precipitates surrounding the grain boundaries in their cast microstructures. This limits the use of high manganese steels as castings in engineering applications requiring high ductility and high toughness. For this reason, the Fe-Mn-C phase diagram should be kept at temperatures above the Acm line for a certain time depending on the section thickness and then subjected to quenching heat treatment in a way that does not allow time for carbide precipitation. As a result of this process, a face-centered cubic structure with 100% austenitic structure and high toughness is obtained [2, 7-9].

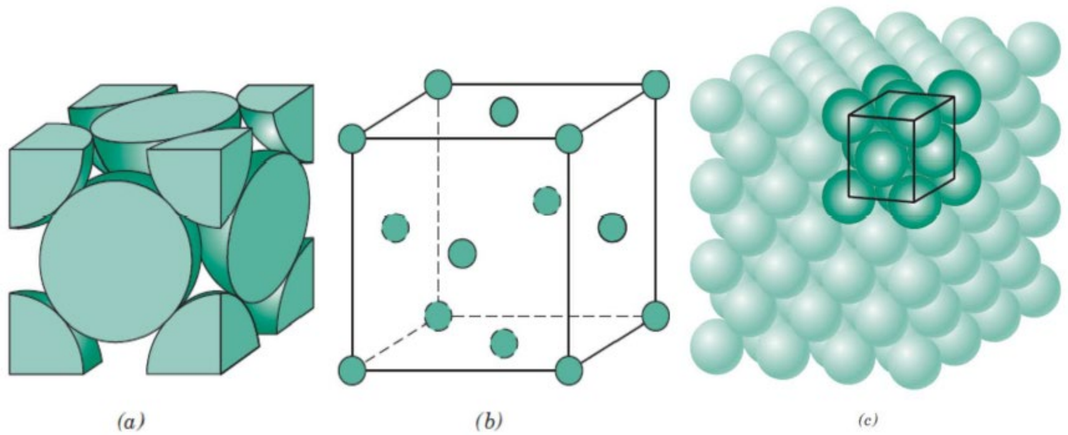

Figure 2: Face-centered cubic structure representation, (a) Solidsphere unit cell representation (b) (in terms of visibility of where all atoms are located) small sphere unit cell representation, and (c) a volume formed by a group of atoms and the unit cell representation in one corner of this volume [29]

In addition to their austenitic internal structures, high manganese steels become resistant to wear by showing work hardening when exposed to mechanical effects. The most important deformation mechanisms that cause strain hardening in these steels are stress-induced martensitic transformation known as Transformation Induced Plasticity influence, mechanical twinning known as Twinning Induced Plasticity influence, dislocation shift and dynamic deformation aging. The different deformation mechanisms in these steels depends on the stack failure energy (SFE) value. Because SFE is the most important parameter that determines the type of deformation mechanism. Therefore, calculation of stack failure energy value and Martensite start temperature is essential for the correct pre-production design of austenitic manganese steels [6, 10, 13, 16].

The TRIP effect is not seen in standard Hadfield steels due to the high carbon and high manganese content. This situation can only be seen in the surface areas due to the low austenite stabilization of the parts that are kept for long periods at high heat treatment temperatures and carbon reduction due to the decarburization effect on the surface. These steels are mostly deformed by classical dislocation shift and TRIP effect as well as twinning within the grain. They show high hardening properties due to the fact that the formed twin boundaries prevent dislocations such as grain boundaries. Therefore, in critical engineering applications where impact wear or metal-to-metal friction occurs, high-strength and wear-resistant austenitic manganese steels are preferred instead of brittle cast irons with high surface hardness [6, 14, 15].

1.2.2. Effect of Alloy Elements

1.2.2.1 Carbon (C)

Carbon is one of the most important alloying elements for high manganese steels. It is generally kept between 1-1.40% in high manganese steels. Since the addition of carbon creates solid solution hardening, it increases the strength values, while it causes a decrease in the toughness values after a certain amount and reduces the weldability. It has a slight but significant effect on yield strength; a decrease in carbon content causes a decrease in yield strength. The main purpose of adding carbon is to increase wear resistance. Because most manganese steels work under high impact. Therefore, it is very important to use the carbon to the highest possible level at which it can be retained in solution after quenching. In this way, a significant improvement in the wear performance of austenitic manganese steels can be achieved. With increasing carbon ratio, tensile strength, yield limit, strength properties and hardness increase in steel, while thinning, elongation at break and notch impact strength decrease. Figure 3 shows the effect of increasing carbon content on mechanical properties [6, 17, 19].

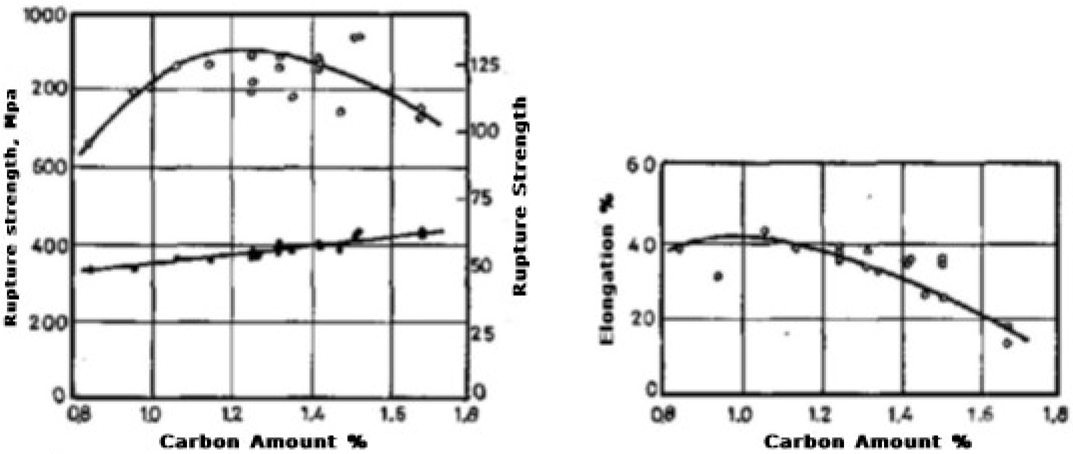

Figure 3: Effect of increasing carbon content on mechanical properties [2]

1.2.2.2 Silicon (Si)

Silicon is used for deoxidation and is not considered an alloying element. It is a carbide-forming element and added to raise the hardness and wear behavior of steel. In general, the best fluidity and casting properties are obtained in manganese steels with the addition of 0.8% by weight silica. Addition of excessive amount of silica causes brittleness of the part. For this reason, according to international standards, the silica ratio is generally limited to 1% and the decision of how much to add usually varies depending on the experience of the manufacturers. It has a strong tendency to segregate during solidification. It increases the carbon activity and lowers the carbon solubility in the austenitic matrix. Figure 4 shows the effect of increasing silica amount on mechanical properties. As can be seen, the addition of silicon up to 1% by weight increases the yield strength, tensile strength and hardness of high manganese steels, while decreasing their ductility due to the formation of micro-structured SiC particles [6, 18, 20].

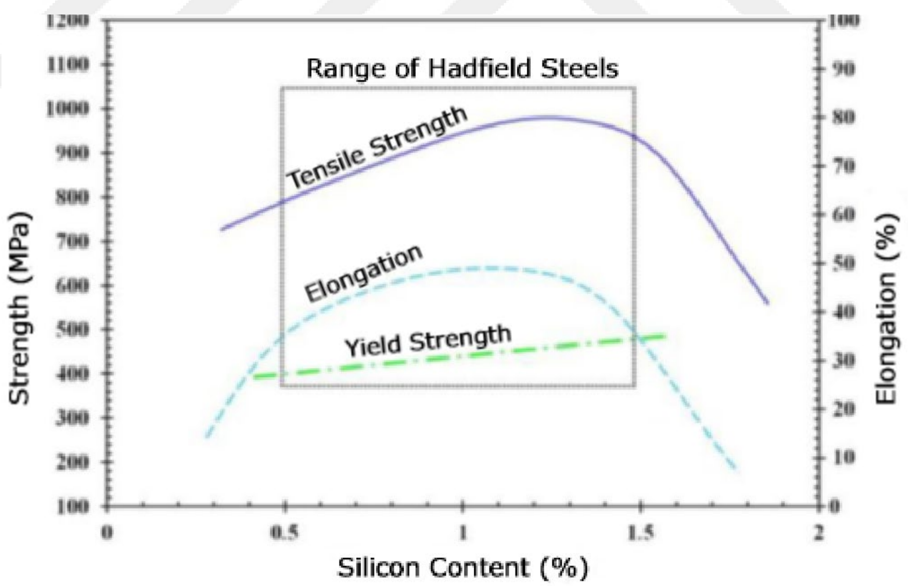

Figure 4: The effect of increasing silicon amount on mechanical properties [2]

1.2.2.3 Manganese (Mn)

Manganese strongly stabilizes austenite. It prevents the conversion from austenite to ferrite and ensures that the microstructure remains 100% austenitic at room temperature after quenching. In other words, manganese is added to prevent the formation of martensite structure that causes hardening and brittleness in the structure and to obtain a homogeneous austenite microstructure [6, 18].

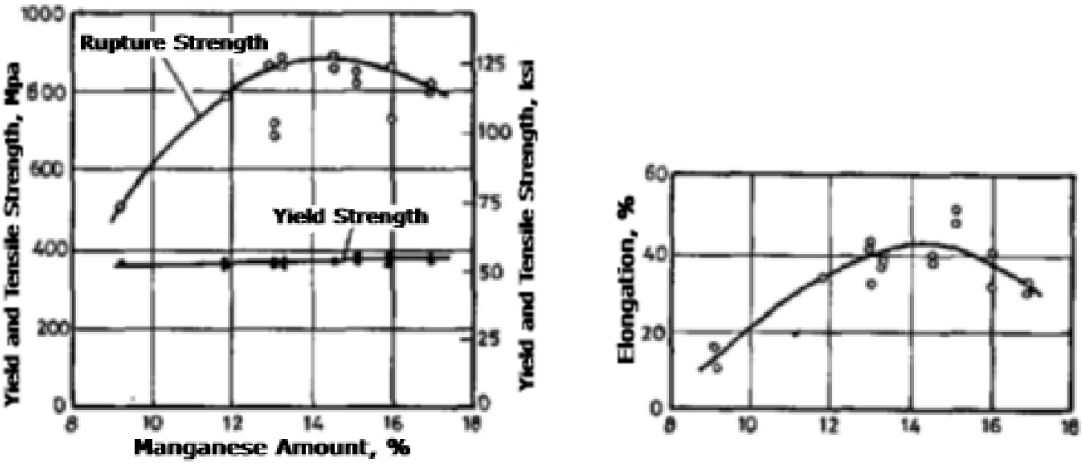

Figure 5: Effect of increasing manganese content on mechanical properties [2]

1.2.2.4 Phosphorus (P)

When phosphorus rises above 0.02% in manganese steels the probability of intergranular cracking increases. Phosphorus above 0.06% rapidly reduces the high temperature plasticity of manganese steel, but the amount of hot tearing becomes greater. Phosphorus below 0.06% only increases the hot tearing tendency [6, 18].

The highest possible phosphorus percentage in the casting depends on the size of the casting, its design, and the magnitude of the stress, which varies with the location and size of the feeders. It is recommended that the phosphorus ratio be below 0.04% for geometrically high wall thickness and hard to cast parts [6, 18].

1.2.2.5 Sulfur (S)

Sulfur is rarely a factor in austenitic manganese steels because of this cleaning effect of manganese added to alloy or unalloyed steels to slag or form the MnS compound that spheroidizes the residues. While the elongation of these residues leads to directional properties in mass steels, they are considered harmless in casting steels [6].

1.2.2.6 Chromium (Cr)

Chromium is added to high manganese steels between 1.5 and 2.5 wt% to increase yield strength and wear resistance. Chromium causes the formation of 23C6 complex carbides in the grain interior and grain boundaries (Fe, Mn, Cr), which reduces the toughness. Since chromium is a strong carbide-forming element, it creates complex (Fe, Mn, Cr)$_3$C$_6$ carbides, causing an increase in hardness in high manganese steels [6].

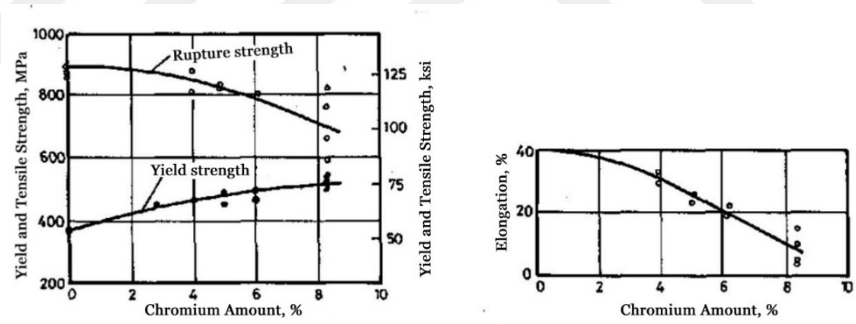

Figure 6: The effect of increasing chromium content on mechanical properties [2]

1.2.3. Usage Areas

These steels are widely used as durable alloys in underground work equipment, where they are subject to great wear, such as grinding mill linings. Hadfield steels have been used successfully where high wear resistance, moderate ductility or strength are required [18].

High manganese steels are steel types used in mining, mineral extraction, ore preparation, train tracks for many years thanks to their superior wear properties. It‘s deformation hardening feature under impact has increased its use in these industrial areas. High-manganese steels, which have high toughness and resistance to wear, have been used in different sectors in order to prevent environmental pollution, changing needs and developing technology over time. The main one of these sectors is the automotive sector [19].

The use of high manganese steels is increasing in absorbing noise and seismic waves. In recent years, due to high seismic activity in countries experiencing frequent and severe earthquakes, various seismic vibration control and seismically isolated structures have been increasingly developed and used in buildings. The desired properties of these steels differ markedly from those of construction steels. Because it has been shown that unpredictable damages can be caused to structural elements by large aftershocks that may occur frequently after high-magnitude earthquakes and large primary earthquakes. A new high manganese steel damping alloy with low cycle fatigue resistance has been developed. High manganese steel named Fe–15Mn–10Cr–8Ni–4Si based on the Fe–Mn–Si shape memory alloy system, which exhibits plastic strain recovery with ε-martensitic transformation due to deformation upon loading and transformation to austenite on subsequent heating has been enhanced. These high manganese steels with low cycle fatigue life have found practical use as long-term seismic dampers in a 40-story skyscraper in Japan. It has been determined that it has an excellent fatigue life compared to 304 quality stainless steel at temperatures between 100 and -20 °C [19].

X120Mn12 high manganese steel, also known as Hadfield steel, is used in mine transport trucks, ore preparation equipment, ore crushers where it is required to provide resistance to abrasion. It is used as drilling rotary excavator, mining balancer device, sieve, bucket, dredger scrapers, mine transport wagon. Thanks to its long life in construction and heavy vehicle equipment, it has a great potential in terms of use. Thanks to their ability to harden during impact, they have a high potential to be used in the manufacture of iron bars, house locks and safes in prisons [19].

Thanks to its high impact toughness, high manganese steels have a high potential to be used as armor steel in the defense industry. Conventional armor steels are designed to shatter lead due to their high hardness during lead response. This causes these parts to also pose a danger. The shattered bullets act like shrapnel. High manganese steels absorb the energy of the bullets thanks to their high toughness. For this reason, it is thought that high manganese steels can replace the traditional armor steels used by tanks, armored vehicles, and bank money transport vehicles. Figure 7 shows the damping of bullets by high manganese steel used as armor steel. In addition, high manganese steels that do not show post-weld phase transformation do not experience post-weld hardening. Additional protection equipment is used to protect traditional armor steels, which become brittle due to hardening after welding, against possible impacts. Thanks to the use of high manganese steels, the use of additional protection equipment will be reduced, reducing both the cost and the weight of the vehicle. Reducing vehicle weight in armored vehicles is also an important issue. With the decrease in the weight of the vehicle, the armored vehicle will have the opportunity to move faster, and it will both save fuel and have the capacity to carry more personnel or equipment. "Perforated steel" is used to reduce vehicle weight. Thanks to the high impact toughness of high manganese steels, this type of steel can also save weight. Because, in order to reach the impact toughness values of high manganese steels, it is necessary to use thicker perforated steel. This is an important factor that increases vehicle weight [19].

Figure 7: A High Manganese Steel showing bullet damping [19]

Some uses of high manganese steels are as follows;

- In mineral processing and grinding mills equipment,
- In water pump shafts,
- In chains and gears (straight + helical),

- In piston pins,
- In valve and camshafts,
- In piston rings,
- In tractor axle shafts and grader blades,
- In shaking sieves,
- In glass cutting discs,
- In mill lining balls and blades,
- In screw guides,
- In gearboxes,
- In auto transmission, camshaft gears,
- Spring reel manufacturing etc. in the fields,
- In oil well exploration equipment,
- Wagon, wear plate and shoes etc.

1.3. General Information and Application Areas of Super (Master) Alloys

1.3.1. General Information

The versatility of superalloys is due to their combination of high strength at high temperature with ductility at low temperature and excellent surface stability. They are alloys used in applications where more severe mechanical stresses and high surface stability are required compared to other applications developed for high temperature applications. A review of the performance of superalloys to increase fuel efficiency and reduce emissions in modern turbine systems reveals the superiority of these alloys for high temperature applications. The hardness of superalloys can be increased after cold deformation, but this hardness may not withstand high temperatures. Superalloys have high strength not only due to the nature and chemistry of the face-centered cubic matrix in austenitic structure, but also due to the effect of precipitate-forming hardening phases. [30].

During the selection of any application area of superalloys; Mechanical properties such as strength, creep strength, fatigue strength, formability and surface stability should be considered. Chemical composition and microstructural variables that are beneficial for one of these properties may have undesirable consequences for the other. For example, fine grain structure is the desired microstructure for low temperature tensile strength, fatigue strength and high temperature formability, while it negatively affects creep strength. Similarly, while high chromium content increases oxidation and hot corrosion resistance in nickel-based alloys, it also causes a decrease in tensile and creep strength, as well as the formation of σ phase. In addition, alloys that are more resistant to temperature are more prone to brittleness, so they can only be shaped using the casting method or produced by powder metallurgy [30].

1.3.2. Usage Areas

Today it also includes aircraft and industrial gas turbines, rocket engines, chemical industry and oil plants. A study of the performance of superalloys to increase fuel efficiency and reduce emissions in modern turbine systems reveals their superiority for high temperature applications [30].

The usage areas of superalloys can be listed as follows:

- Aircraft/industrial gas turbine parts: discs, bolts, shafts, aircraft propellers, blades, combustion chambers, afterburners, thrusters,
- Steam turbine power plant parts: bolts, propellers, flue gas supplementary heaters,
- Automotive parts: turbo compressors, exhaust valves,
- Metalworking material: high temperature resistant work tools and dies,
- In medical equipment: dentistry,
- Space shuttle parts: on aerodynamically heated surfaces, rocket engine parts,
- In heat treatment parts: clamping equipment,
- In the chemical and petrochemical industries: used in bolts, valves, pipes, pumps, etc..

1.4. Research Objectives and Tasks

The significance of this research is to investigate the effects of Al5Ti1B on the microstructure and mechanical properties of high-manganese steels fabricated by casting method. The research missions can be characterized as follows:

The topics covered in this thesis are covered in five different chapters.

I. In Part 1, the general content of the study, the intended subject, the purpose of the thesis, the general content of the tests and analyzes to be made are mentioned.
II. In Chapter 2, the literature review of the subjects, tests and studies that will be examined in this thesis has been examined.
III. In Chapter 3, the production processes, manufacturing techniques, tests and analyzes of the samples produced within the scope of this thesis and the way they are made are mentioned.
IV. In Chapter 4, the results of the tests and analyzes carried out within the scope of this thesis and the effect on the mechanical properties of the material are given.
V. Chapter 5 is discussed by summarizing all the results obtained.

CHAPTER 2
LITERATURE SURVEY

A literature review on the production of high manganese steels, the examination of microstructure and mechanical properties is presented in this section.

Gürol [2], in the doctoral thesis, investigated the effects of carbon, manganese and titanium elements in the composition of high manganese steels, as well as the effects of different heat treatment and casting temperatures on microstructure and mechanical properties, and under suitable microstructure conditions, tensile strength, impact resistance and abrasion resistance aimed at improving its features. First, it was aimed to determine the optimum carbon and manganese ratio together with the optimum solution temperature by using casting samples produced in different chemical compositions at a constant casting temperature (1450 °C). Compared to the reference alloy (1.0C-13Mn); 5% improvement in yield strength, 19% improvement in elongation and 21% improvement in impact strength were obtained as a result of solution heat treatment of 1.0C-17Mn sample at 1100 °C. In the second stage of the experimental studies, the effect of Ti addition at different rates was examined. As a result of the study, it was observed that the stable Ti(CN) phase was formed in the microstructure with the addition of titanium, and accordingly, there was a 45-52% reduction in grain size. Despite the 22% decrease in impact strength due to differences in Ti(CN) distribution and morphology, the most ideal results were 1.0C-17Mn-0.05Ti specimen with 7% increase in tensile strength, 9% increase in elongation and 40% increase in abrasion resistance was obtained. In the last stage of the study, real track shoe (3.5 tons) parts were cast with an alloy with 1.0C-17Mn (without Ti) composition. The effects of different casting temperatures on microstructure and mechanical properties were investigated. Significant differences were observed between the data obtained from the samples in the experimental studies and the thick-section cast part in terms of mechanical and microstructural properties. In the face of the increase in casting mass and thickness, the desired mechanical properties were obtained in the casting produced at lower casting temperatures (1420 °C). Thus, he found that both chemical analysis and heat treatment and casting temperature greatly affect the performance of high manganese steels. As a result, the production of cast parts used in the industry with appropriate casting parameters has increased the service life of the parts by 30%.

In a study, Dastur and Leslie [10] investigated that Hadfield manganese steel in the single-phase austenitic state exhibits jerky (jagged) flow and the flow exhibits negative (reverse) strain rate dependence when stressed in tension in the temperature range of -25 to 300 °C. They noted that the hardness is effected from the twinning process and temperature. The known effect of Mn on carbon activity and previous internal friction studies of HMSs cause to the conclusion that dynamic strain aging by reorientation of carbon members of C-Mn pairs, rapid machining in Hadfield steel is the main cause of hardening.

In another study, Aytekin [7] reviewed the metallographic structures of (Fe-Mn-C) alloys in equilibrium and in practice, after summarizing the uses and amounts of manganese in steels; indicated the location and importance of high manganese austenitic steels among them. The macro- and micro-structures, heat treatments and mechanical properties of manganese austenitic steels cast in molds with production, casting and welding techniques were examined and the most suitable application areas were determined accordingly.

Mahlami and Pan [3] argued in their study that Hadfield steel had a large capacity for work hardening on impact and was often used for railway components. In this article, Mahlami and Pan provided a comprehensive analysis of the overall appearance of high manganese steel HMS casting. An appropriate HT process was commented, and the mechanical properties of the steel and the work-hardening rate were also discussed in order to know which steel is best suited for which application.

In a study which was carried out by Kayadelen [1], changes in hardness, impact resistance and especially wear properties of new structures obtained by adding Vanadium and Molybdenum to high manganese austenitic steels were observed. It added Vanadium and Molybdenum at a rate of 1% by weight. Besides the reference sample, by adding 1% Vanadium to the reference sample and 1%

Molybdenum to the reference sample, 6 samples were created in 3 different groups. The samples were first prepared for casting. The samples, whose castings were completed, were kept at 1200 °C for 24 hours and then cooled to room temperature. The cooled samples were surface treated. Impact resistance test was performed on the prepared samples. After performing a total of 9 hardness tests, 3 of each sample, the wear tests were carried out. Within the scope of wear tests, wear tests were performed for each sample under two different load and speed conditions. He used stereomicroscope and XRD for characterization after wear tests. As a result of the experiments, high manganese austenitic steel, which is actively used in the industry, showed increases in impact resistance, hardness and wear resistance criteria as a result of the applied processes. It was observed that the Vanadium added sample gave better results in impact resistance tests, and the molybdenum added sample gave better results in hardness and wear resistance.

Sabzi et al. [21] in their studies, Hadfield investigated the production processes and properties of HMSs. The structure for this steels should be austenitic single-phase to provide optimum toughness. Mn is a carbide-forming element and formed Mn_3C and $(Fe,Mn)_3C$ in the steels. Twin stress contributed greatly to the plastic deformation ability of the steel and is well known that the steels have low wear resistance.

In a study, Turhan [18] examined the hardness of austenitic hard manganese steels (12-14% Mn, 16-18% Mn) by impact and the resistance of the formed martensite layer against abrasion and compared them with the literature. On this occasion, he gave general information about wear and information about wear types. He then made statements about wear-resistant materials and austenitic hard manganese steel. The properties of the test jig were included, then the austenitic steel samples with 14.5% Mn and 16.5% Mn were homogenized at 1030 °C and 1010°C, and some of them were subjected to abrasion at different amounts under constant load, constant time and constant distance. Then he evaluated the results by drawing graphs from the obtained results.

Anijdan et al. [8] investigated the HT process influences on the mechanical properties of Hadfield steels. I was seen that the fatigue life of the samples quenched in the salt bath which showed the lower Mn_3C precipitates was longer than the sample quenched in pure water.

Erdem [17] investigated the wear behavior of nine samples in an abrasive environment as three different materials with different heat treatments. The samples, which were brought to the appropriate dimensions for the experiment on the milling machine, were then subjected to heat treatments for the experiments. He examined the microstructure photographs of each sample and compared the obtained microstructures. Afterwards, these heat-treated samples were subjected to the abrasive wear test. As a result of these tests, it has been determined that there is a direct relationship between the wear behavior and mechanical properties of the materials that are the subject of the study. It has been observed that with the improvement of the mechanical properties of the materials, their wear resistance also increases. It has been observed that the wear resistance of the materials subjected to normalization annealing decreases, while a good wear resistance is provided in the materials that are subjected to hardening. As a result of the studies, it has been seen that the wear resistance is lower in low carbon steels. However, with the addition of alloying elements such as chromium and manganese to the material, it has been able to improve the wear resistance.

Venturelli et al. [14] investigated the effect of the grain refinements on the Hadfield steels. The grain size of the steels reduced with the addition of the grain refinements from 3000 µm to 600 µm. The process improved the mechanical properties of the steels by the plastic deformation rate of the twinning mechanism.

Zuideme et al. [11] conducted a study on the hardening and wear behavior of Al-modified Hadfield Mn steels with a composition ranging from 1 % to 1.75 % C and 0.0% to 4.0% Al. The additions of aluminum increased the metastable solubility of C in the steel by reducing C activity and diffusivity in Hadfield austenites. Additions of aluminum prevented the twinning and consequently raised the SFE of austenite.

Mahlami et al. [15] argued in this study that High manganese steel, when used under the primary crushing system, exhibits superior wear resistance when used under the secondary and tertiary crushing modes. The study presented the influence of V content on the mechanical properties and microstructure evaluation of HMSs.

The vanadium advanced the wear and hardness proeprties by forming vanadium-carbides.

Pham et al. [21] investigated the effect of V content on the grain size and hardness of a HMS such as $Mn_{15}Cr_2$. To a degree, vanadium improved the hardness and decreased the grain size. HMS containing 1% vanadium had the highest impact toughness of 115J/cm^2 and the highest Brinell hardness (HB) of 223. The rate of 1% of vanadium was seen to be optimum for the steels to obtaining the maximum hardness and tougness. In addition, TEM analysis showed that after heat treatment, fine V-carbides were dispersed in the steel.

Çıkıt [22] in his own study, high wear resistance of the materials used in the places where it is necessary was examined. Samples belonging to high Cr white cast iron, high Cr steel and HMS material groups and which were subjected to cooling process by three different methods were used. There are four samples in the high Cr white cast iron group, with C amounts of 2.84% and 3.16%, while Cr amounts are 25.8% and 20.2%, respectively. Cooling styles after heat treatment differed in air, oil and fan. There are three samples in the high chromium steels group, the C amounts are 0.4% and 1.53%, while the Cr amounts are 7.38% and 13.4%, respectively. Cooling styles after heat treatment differed in oil and fan. Finally, in the manganese steels group, there are two samples, the C amounts are 1.16% and 1.34%, the Cr amounts are 0.37% and 1.8%, and the Mn amounts are 11.6% and 17%, respectively. Cooling methods after heat treatment are the same in both, water cooling. The aim of this study was to examine the structure, mechanical properties and wear behavior of these materials, which find application in crushers and grinders, as a whole. In experimental studies, metallography samples of each material were prepared for microstructural characterization and microstructural examinations were made on these samples using an optical microscope. He also performed XRD analysis on the samples. Mechanical tests such as hardness, abrasion, tensile, notch impact were also applied to the samples. The fractured surfaces of the samples subjected to the impact test were examined by SEM to determine the fracture characteristics. Found that among High Cr steel, high Cr white cast iron and high Mn steel samples, the highest hardness and best wear resistance were in high Cr white cast iron samples. This result concluded that the continuous chromium carbide network structure in the structure was effective. Ductile fracture occurred only in high Mn steel samples.

While the impact resistance of high Cr steel and high Cr white cast iron samples were in the same order, the impact resistance of high Mn steel samples was quite high. He concluded that the toughness of these materials is better. In high Mn steels, a hard and wear-resistant layer is formed on the surface as a result of cold strain hardening (transformation hardening) under the effect of pressure and impact. Thanks to these properties, the wear behavior of high Mn steel samples improved. On the other hand, it was observed that the strength and wear resistance increased with the increase in the amount of Cr and Mn in high Mn steel samples. The highest tensile strength was reached in the high Cr steel sample with the highest Cr/C ratio. In the samples with the same chemical composition, better hardness-wear resistance-impact strength values were obtained in the samples cooled in oil after heat treatment. As a result of all the experimental studies, while recommending the use of high Cr white cast iron materials where high wear resistance is required; in cases of impact wear, high Mn steel materials are preferred.

CHAPTER 3
EXPERIMENTAL PROCEDURE

In this section, the production stages of high manganese steel samples produced by the sand mold casting method by adding Al5Ti1B and the materials used during the production stages are mentioned. In addition, the experimental studies on the post-production samples and the devices and equipment used during these studies are explained.

3.1. Production of Samples by Sand Casting Method

In this thesis study; Super (master) alloy Al5Ti1B (Altibor) has been added at different rates to GX120Mn13 and GX120Mn17 High Manganese Steel Castings with high wear resistance, which are frequently used in industries such as Crushing, Mining, Cement. The Chinese origin Altibor material has been purchased from Bilginoğlu Company, which is operating in Turkey, buying raw materials from abroad and making sales in Turkey; the spectral analysis results are given in Table 1.

Table 1: Al5Ti1B chemical analysis (wt.%)

Element	Actual Analysis Value	Standard Analysis Range
Si	0.099	0.20 max
Fe	0.066	0.18 max
Ti	4.99	4.50-5.50
B	1.03	0.9-1.1
V	0.013	0.20 max
Sr	<0.03	0.10 max
Mg	<0.10	0.45 max
Other Each	<0.04	
Other Total	0.10	
Al	Remain	

For the production of the sand mold, first of all 1 wooden pattern was made. This model was designed and produced as a Y Block, as seen in Figure 8, in order to avoid shrinkage and slag problems and to be suitable for the tests and analyzes to be made.

In the preparation of the sand mold, a mixture of fine grained 35-40 AFS silica sand (SiO_2), Resin (1.50% of the sand) and Harder (25% of the resin) was used. The picture of the model used in Figure 9 and the post-cast sample of the Y block are given in Figure 10.

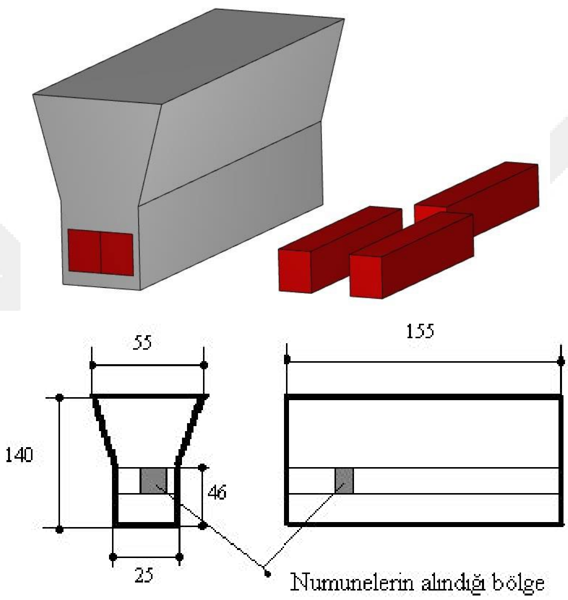

Figure 8: Y block design to be cast (Unit:mm)

Figure 9: Y block wood pattern

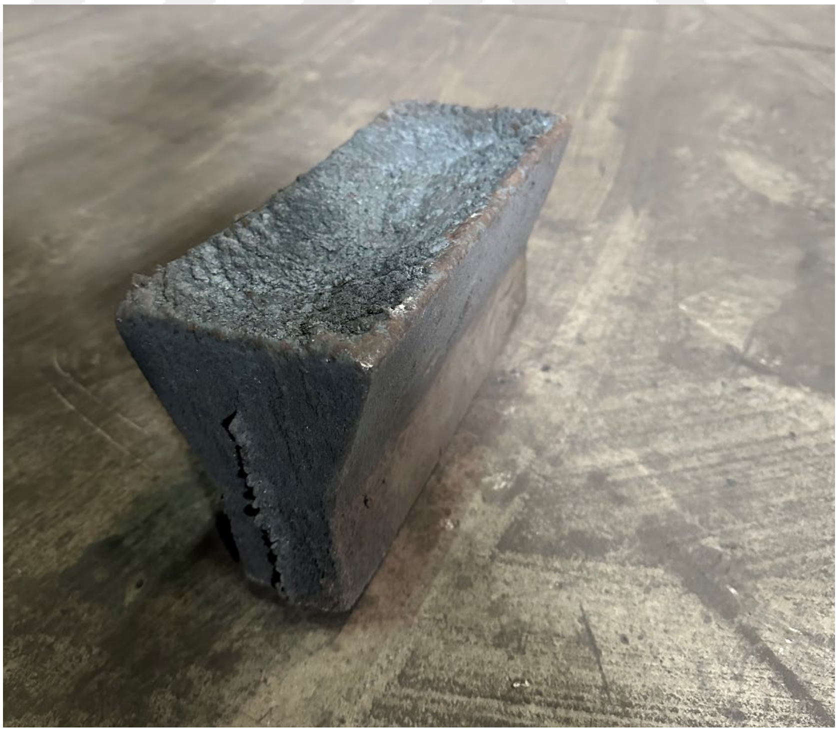

Figure 10: Y block sample with completed casting

The casting process is made of EGES brand EGP1500SE mode induction furnace, schematically shown in Figure 11, with 800kW + 200kW power, 50 Hz frequency, operating with +/- 1°C sensitivity, and 1500 kg melting capacity.

Figure 11: Induction furnace

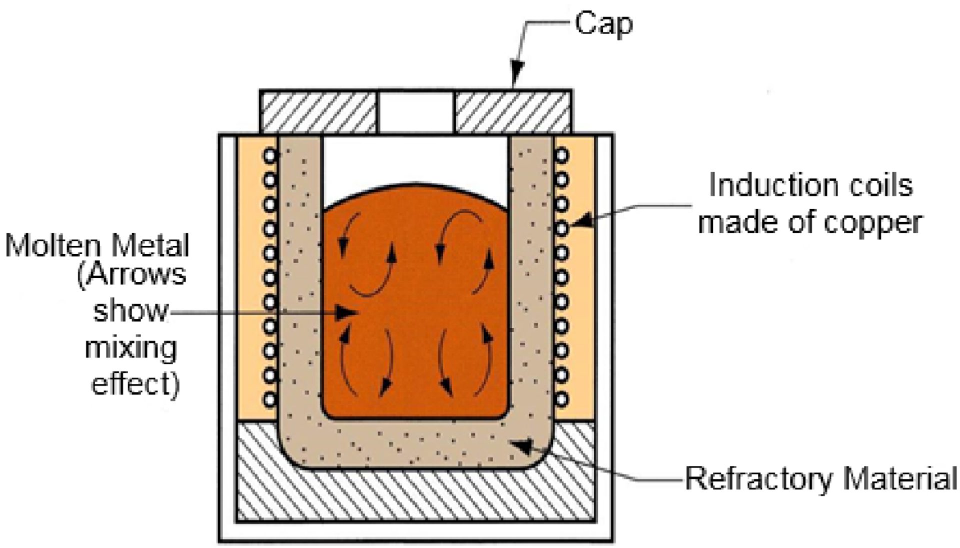

Figure 12: Schematic representation of induction furnace [23]

Each prepared Y block sample was set to pour 15 kg of molten metal into the mold. The melting process started by filling the induction furnace with scrap. After the molten metal in the furnace reached approximately 1200 kg, the desired composition was obtained by adding the ores in the desired analysis. After the liquid metal temperature reached 1420 °C, perlite was added to clean the slag on the melt and the slag formed on the surface of the liquid metal was removed and the melt was cleaned. Then, 15 kg of molten material ready for casting was taken into the ladle.

Figure 13: Liquid metal

Al5Ti1B was added as 0.05%, 0.1%, 0.2%, 0.5% and 1%, respectively, to the melted GX120Mn13 and GX120Mn17 material taken into the crucible. Table 2 shows the standard compositions of GX120Mn13 and GX120Mn17 products. In addition, the amount of Altibor added for 15 kg of molten metal is given in Table 3.

Table 2: Compositions of alloying elements (wt.%)

Material Names	C	Si	Mn	P	S	Cr
GX120Mn13	1.10 - 1.30	0.30 - 0.50	12.00 - 14.00	0.10max	0.040max	1.50 max
GX120Mn17	1.10 - 1.30	0.30 - 0.50	16.00 - 18.00	0.10max	0.040max	1.50 - 1.60

Table 3: Quantities of Al5Ti1B added to alloying elements

Code	GX120Mn13					GX120Mn17				
Samples	**1**	**2**	**3**	**4**	**5**	**6**	**7**	**8**	**9**	**10**
Added Al5Ti1B Amount (wt.%)	0.05	0.10	0.20	0.50	1	0.05	0.10	0.20	0.50	1
Amount of Added Al5Ti1B (g)	7.5	15	30	75	150	7.5	15	30	75	150

High manganese steels are heat treated between 950 – 1100 °C. The purpose of the applied heat treatment is to provide high impact strength to the steel by ensuring that the carbide structures are completely dissolved in the austenite phase and the microstructure completely transforms into the austenite phase after quenching. If cooling is slow, the carbides precipitate and pearlite happens. The graph of the heat treatment process is given below. As can be seen from this graph, the samples were raised to 1050 °C in about 5.5 hours. The samples were kept at 1050 °C for approximately 2.5 hours. Afterwards, the samples were taken from the annealing furnace within a maximum of 30 seconds with minimum temperature loss and immersed in the water pool.

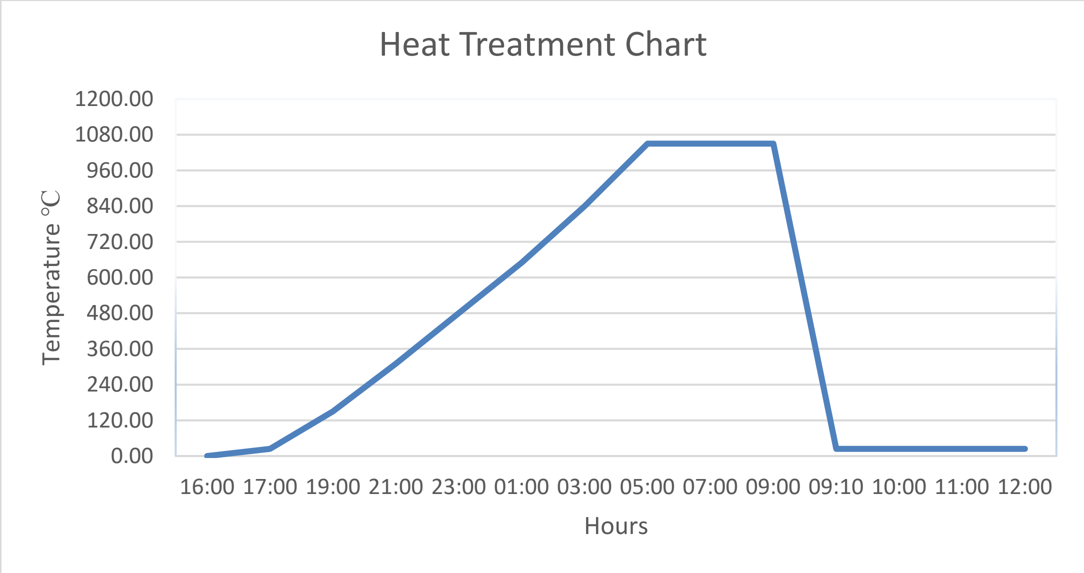

Figure 14: Heat treatment chart

3.2. Spectral Analysis

Spectral analysis was performed to determine the chemical composition of the produced samples. For this, Oxford Instruments brand Foundry-Master Xpert model spectrometer device shown in Figure 15 was used.

Figure 15: Spectral Analysis Device

Before checking the spectral analysis, the sample was polished with the polishing device shown in Figure 16. Then, the samples were placed in the spectrometer in order and their spectral analyzes were examined by incineration.

Figure 16: Sample polishing device

3.3. Optical Microstructure Studies

For microstructure examinations using an optical microscope, first of all, the cast samples were cut in the Metkon brand Servocut302 model device, shown in Figure 17, using cooling liquid. Using a cloud brand polishing device, wet sandpaper was applied at sanding levels between 600 mesh and 1200 mesh, and then it was polished on the cloth using a 6 micron diamond solution. Afterwards, the samples were taken in the Metkon brand Ecopress52 model Bakelite device shown in Figure 18. Macro photographs of the samples that have been mounted are given in Figure 19. Afterwards, the samples were etched in Nital (1-5 ml HNO3 + 99-95 ml Ethyl Alcohol) solution for 10-20 seconds. The etched samples were obtained from Aslankaya Döküm ve Makine San. Trade Inc. Microstructure images were taken using the Nicon brand Eclipse MA100 model inverted metal microscope in the laboratory. The image of the optical microscope used in the thesis study is given in Figure 20.

Figure 17: Sample cutting device

Figure 18: Mounting device

Figure 19: Mounted samples

Figure 20: Specimen examination under optical microscope

3.4. Scanning Electron Microscopy (SEM) Studies

For scanning electron microscopy (SEM), the samples shown in Figure 19 have been polished. It was then mounted and etched. Microstructure images of 10 different samples with specific ratios of Al5Ti1B added (Table 3, Table 4) were taken with the SEM device in Gaziantep University ULUTEM laboratory. The image of this device, which is an emission scanning electron microscope modeled by ZEISS brand GeminiSEM300, is given in Figure 21. SEM analyzes were performed at 100X, 150X and 1200X magnifications, and energy distribution spectroscopy (EDS) analyzes were also performed in this device to determine the elemental composition of regions and points with different contrasts seen in the microstructures.

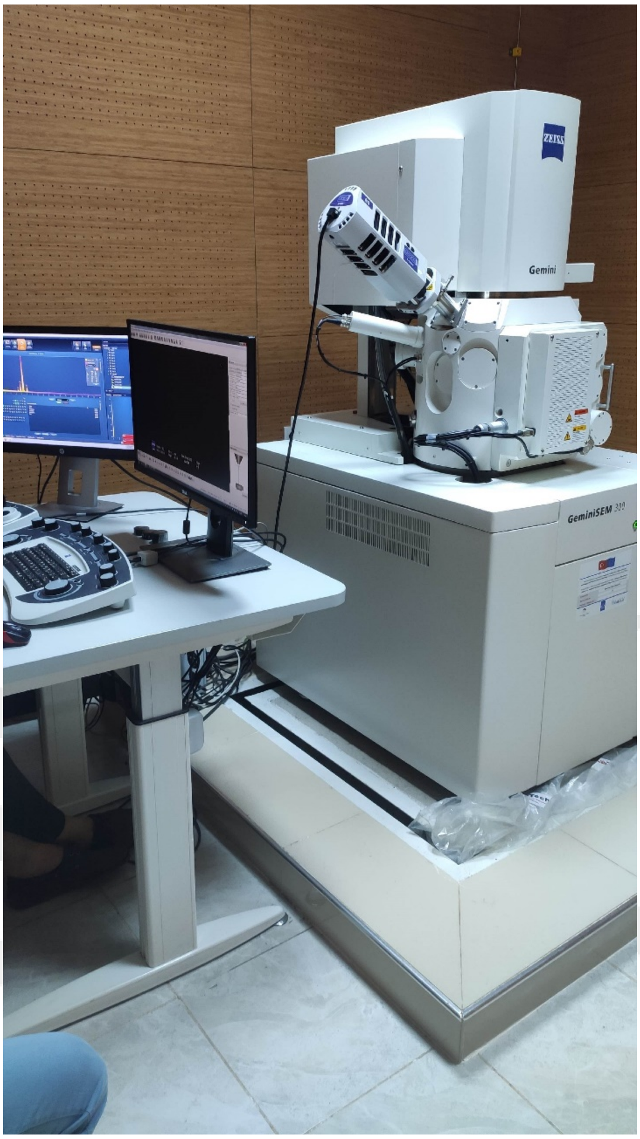

Figure 21: Scanning Electron Microscope - SEM

3.5. Hardness Measurements

Measurement techniques such as Rockwell, Brinell and Vickers are used to determine the hardness values of the high manganese steels produced. Among these, hardness measurements made by Vickers and Rockwell methods are the most used methods [23]. The hardness of the high manganese steels produced within the scope of this thesis was investigated by measuring in terms of Vickers hardness measurement.

The samples to be used for Vickers hardness measurements were wet sandpapered between 600 and 1200 meshes using the Bulut brand polishing device shown in Figure 16, and then they were polished on the cloth using 6 micron diamond solution. The hardness of the polished samples was determined with the Bursam NDT Vickers hardness measuring device shown in Figure 22. Hardness studies were carried out under a load of 1 kg at a time of 10 sec..

Figure 22: Vickers hardness tester

3.6. Wear Tests Application

Abrasion occurs due to undesired material rupture from the surfaces of objects moving relative to each other. This test was carried out in order to determine the abrasion resistance of the prepared samples. The schematic view of the abrasion test device used in the experimental studies is given in Figure 23.

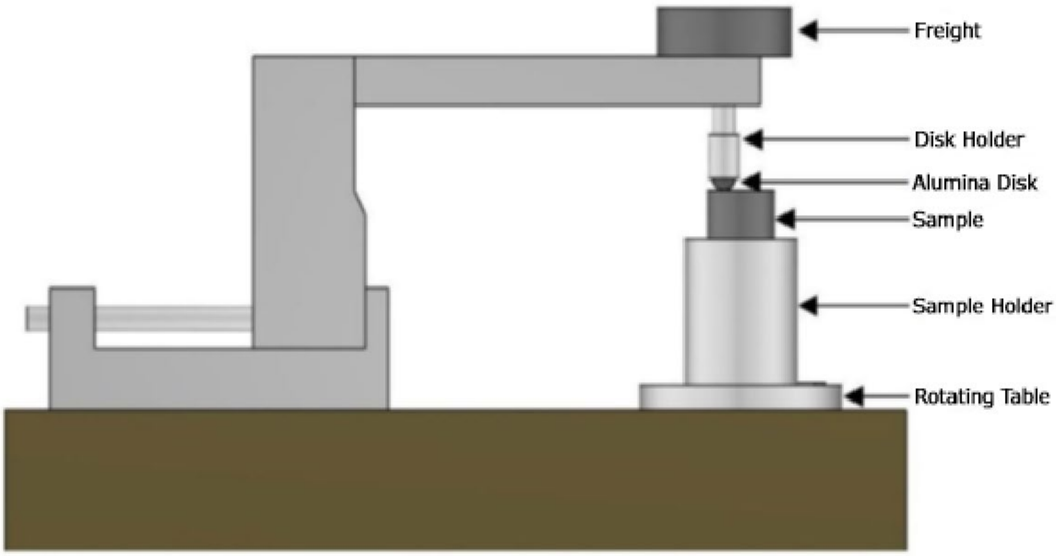

Figıre 23: Schematic view of the abrasion test device used in experimental studies [2]

The wear test was performed on the CSM Tribometer pin-on-disc wear device shown in Figure 24. Wear tests were carried out at a speed of 10 cm/s at 250 m, 500 m and 1000 m sliding distances under 5 N and 10 N loads. In order to determine the weight losses, the samples were carried out on the Sartorius BL 210 S model analytical balance with 0.0001 sensitivity given in Figure 25 after the wear test. Volume losses and wear rates are calculated with the formula given below.

$$Volume\ Loss\ (mm^3) = \frac{Weight\ loss\ (g)}{Density\ (g/mm^3)} \times 1000$$

$$Wear\ Rate\ (mm^3/km) = \frac{Volume\ loss\ (mm^3)}{Sliding\ distance\ (km)}$$

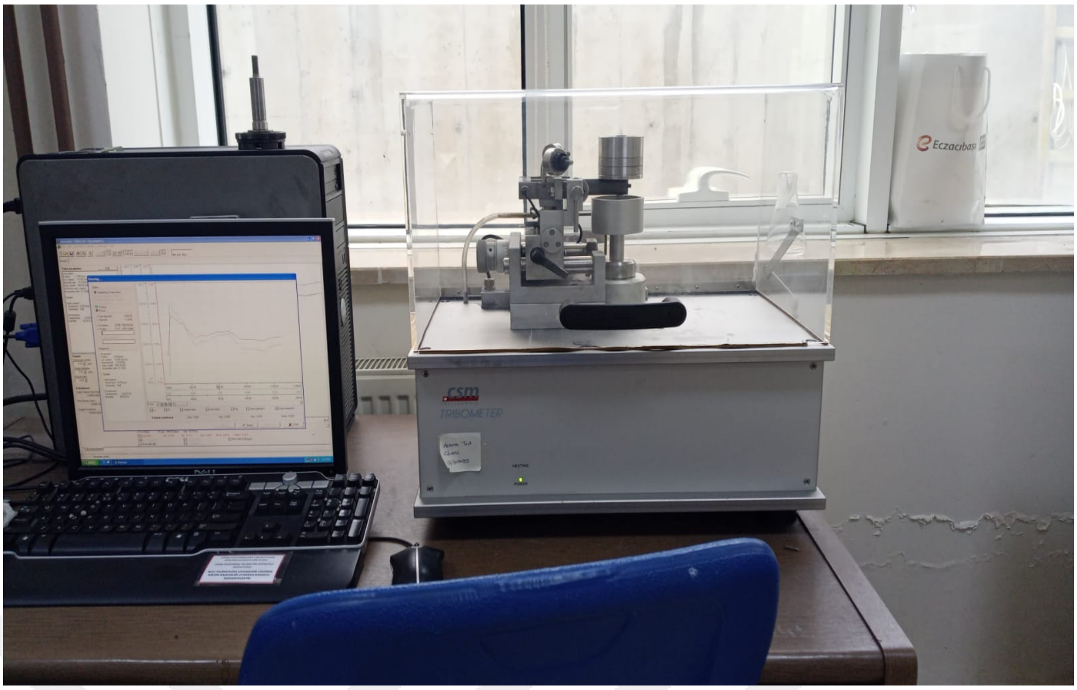

Figure 24: Abrasion tester

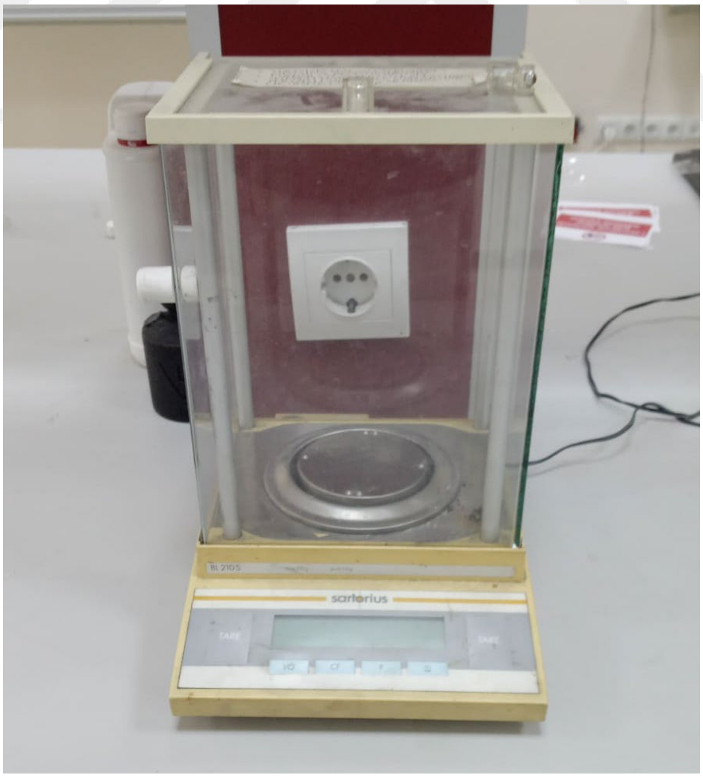

Figure 25: Analytical balance

CHAPTER 4
RESULTS AND DISCUSSIONS

4.1 Spectral Analysis Results

In Table 4 below, the spectral analyzes resulting from the addition of Al5Ti1B to the GX120Mn13 and GX120Mn17 analyzes mentioned in the section 3.1 Production of Samples by Sand Casting Method are given. The presence of Aluminum and Titanium in high manganese steels increased with the addition of Al5Ti1B. Boron element is less than 1 Angstrom in size, so it could not be detected by the current method. It was concluded that the addition was successful according to the spectrometer results

Table 4: Spectral analyzes after Al5Ti1B addition to GX120Mn13 and GX120Mn17 (wt.%)

Alloy	Al5Ti1B	C	Si	Mn	P	S	Cr	Al	Ti
GX120Mn13	**0.05**	1.2800	0.4700	12.8000	0.0580	0.0170	1.5500	0.0077	<0.0005
	0.10	1.2500	0.4530	12.8000	0.0550	0.0160	1.5100	0.0105	<0.0005
	0.20	1.2200	0.4490	12.7000	0.0450	0.0140	1.4600	0.1050	<0.0005
	0.50	1.2500	0.4630	13.2000	0.0510	0.0130	1.5900	0.1970	<0.0005
	1.00	1.2900	0.6370	13.5000	0.0560	0.0040	1.6800	>0.3000	0.0304
GX120Mn17	**0.05**	1.2400	0.4940	18.8000	0.0410	0.0070	2.2700	0.0032	<0.0005
	0.10	1.2500	0.5290	18.5000	0.0440	0.0090	2.2700	0.0343	<0.0005
	0.20	1.2700	0.5300	18.2000	0.0460	0.0110	2.2800	0.0609	<0.0005
	0.50	1.2800	0.5210	18.3000	0.0470	0.0100	2.2800	0.2000	<0.0005
	1.00	1.2500	0.5150	18.1000	0.0470	0.0110	2.2600	>0.3000	<0.0083

4.2 Microstructure Results

4.2.1 Optical Microscope Results

In Figure 26 and Figure 27 a-e, optical microscope images of GX120Mn13 and GX120Mn17 samples, to which Al5Ti1B was added at different rates, are given, respectively. Austenite-perlite matrix formation was observed in the samples. However, it was observed that the main phase austenite phase was present in all samples. It was observed that hard carbides precipitated at the grain boundaries were formed. Optical microscope images were confirmed by scanning electron microscopy and electron dispersion spectrometry results. The addition of Al5Ti1B to the chemical composition of the steels resulted in larger austenite grain size, reducing the amount of precipitate and promoting the formation of carbides and pearlitic structure.

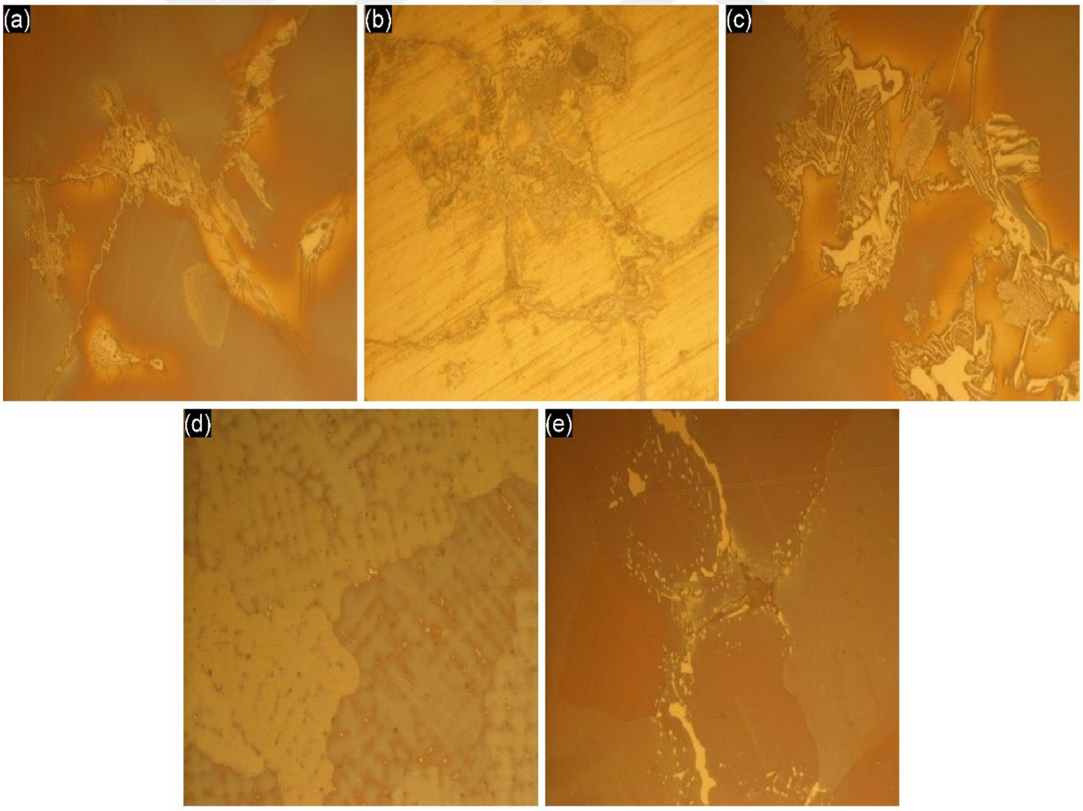

Figure 26: Microstructure images of samples under x50 magnification in addition of Al5Ti1B to GX120Mn13 material

a.GX120Mn13-%0.05, **b.**GX120Mn13-%0.1, **c.**GX120Mn13-%0.2, **d.**GX120Mn13-%0.5, **e.**GX120Mn13-%1

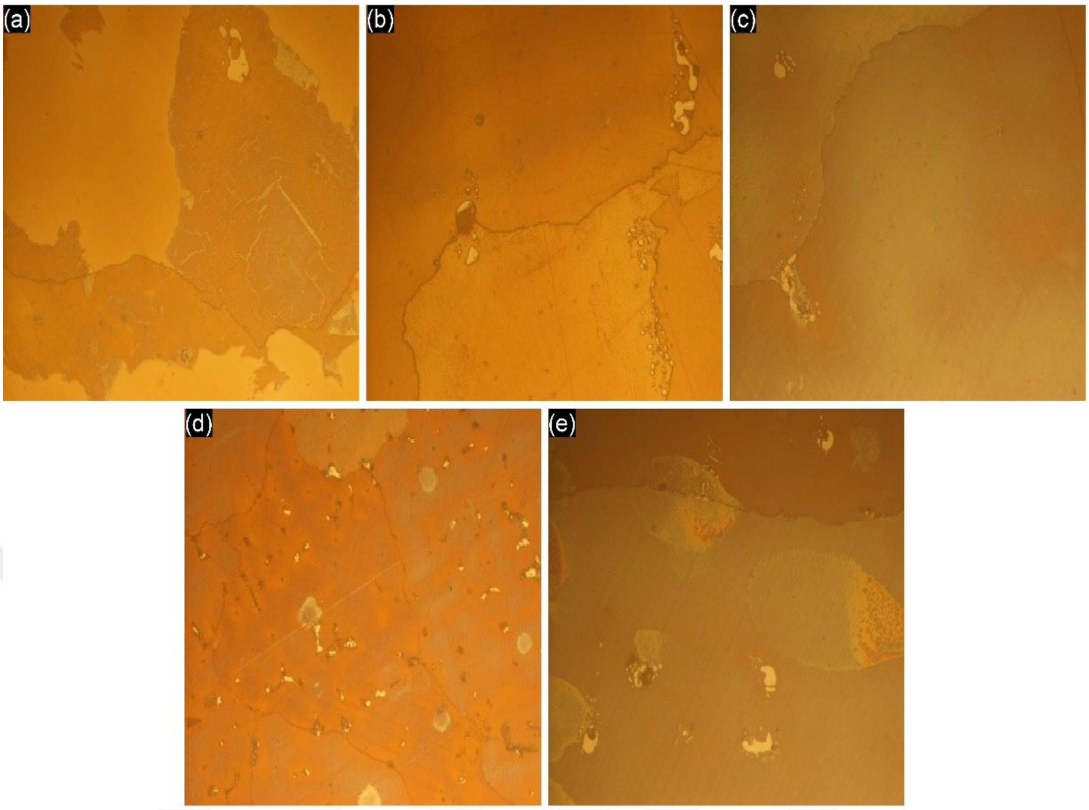

Figure 27: Microstructure images of samples under x50 magnification in addition of Al5Ti1B to GX120Mn17 material

a.GX120Mn17-%0.05, **b.**GX120Mn17-%0.1, **c.**GX120Mn17-%0.2, **d.**GX120Mn17-%0.5, **e.**GX120Mn17-%1

4.2.2 Scanning Electron Microscopy (SEM) Results

In the figures below, scanning electron microscope images of GX120Mn13 and GX120Mn17 samples with different ratios of Al5Ti1B addition are given, respectively. Austenitic-pelitic microstructure formation was observed in the samples. In other words, it consists of inhomogeneous perlite-like lamellar carbide particles precipitated along the grain boundaries together with the austenitic matrix. It was observed that hard carbides precipitated at the grain boundaries were formed. Hard carbides are considered to have a spherical structure. Optical microscope images and scanning electron microscopy images were found to be in good agreement.

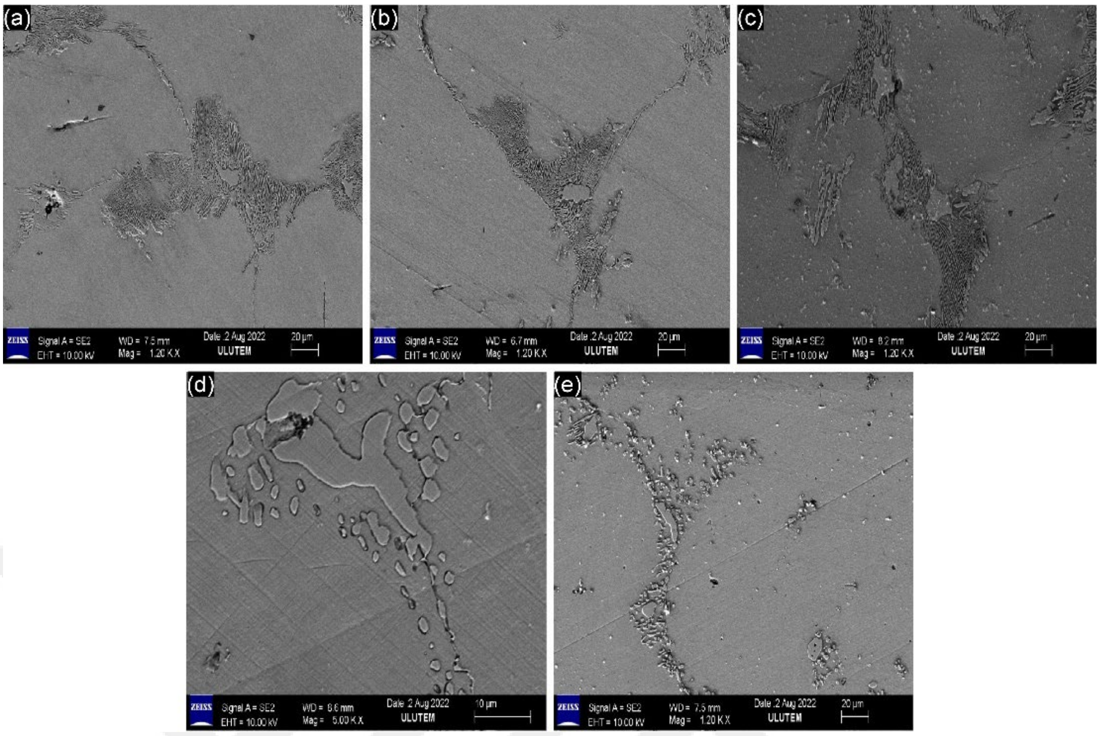

Figure 28: SEM images of samples in addition of Al5Ti1B to GX120Mn13 material

a.GX120Mn13-%0.05, **b.**GX120Mn13-%0.1, **c.**GX120Mn13-%0.2, **d.**GX120Mn13-%0.5, **e.**GX120Mn13-%1

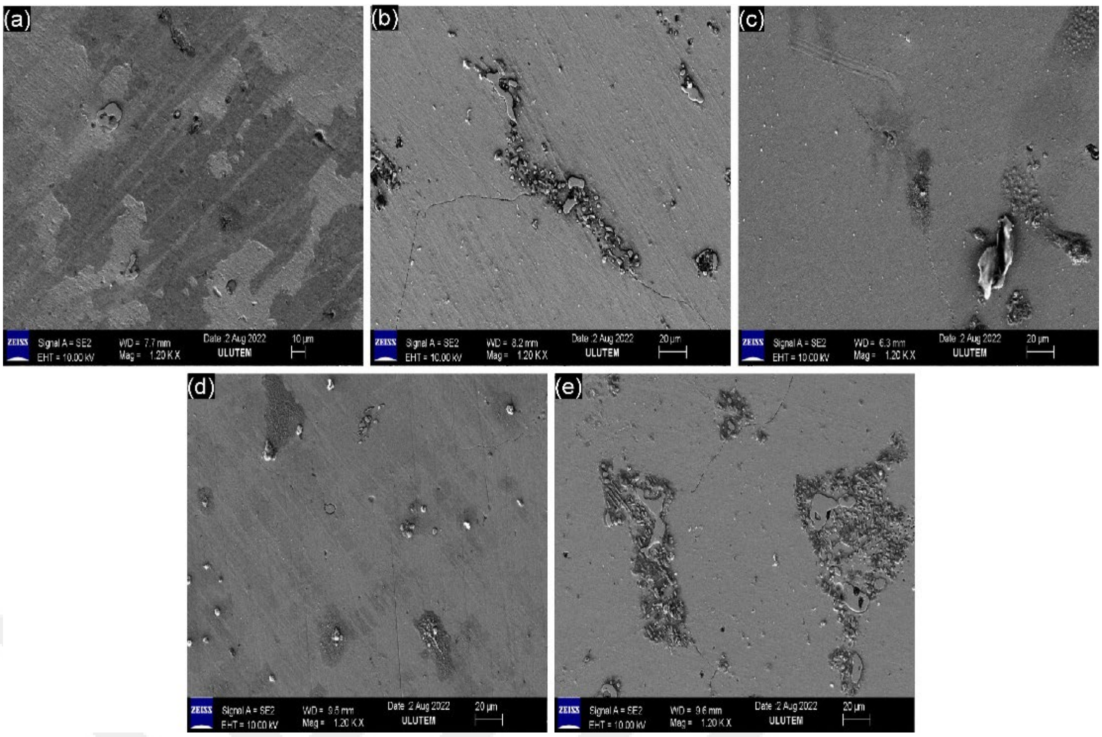

Figure 29: SEM images of samples in addition of Al5Ti1B to GX120Mn17 materials

a.GX120Mn13-%0.05, **b.**GX120Mn13-%0.1, **c.**GX120Mn13-%0.2, **d.**GX120Mn13-%0.5, **e.**GX120Mn13-%1

4.2.3 EDS Results

In the figures below, the electron distribution spectra of the samples from different points are given. The presence of added master alloys in the spectra has been confirmed and it is seen to be in agreement with the spectral section data. It is also seen in the elements of the formation of hard carbides. The microstructure of cast high manganese austenitic steel includes some austenitic and grain boundary carbides $(Fe,Mn)_3C$. These carbides are complex and precipitate especially at the austenite grain boundary. In other words, carbides form and precipitate along austenite grain boundaries due to slow cooling during the solidification process [24].

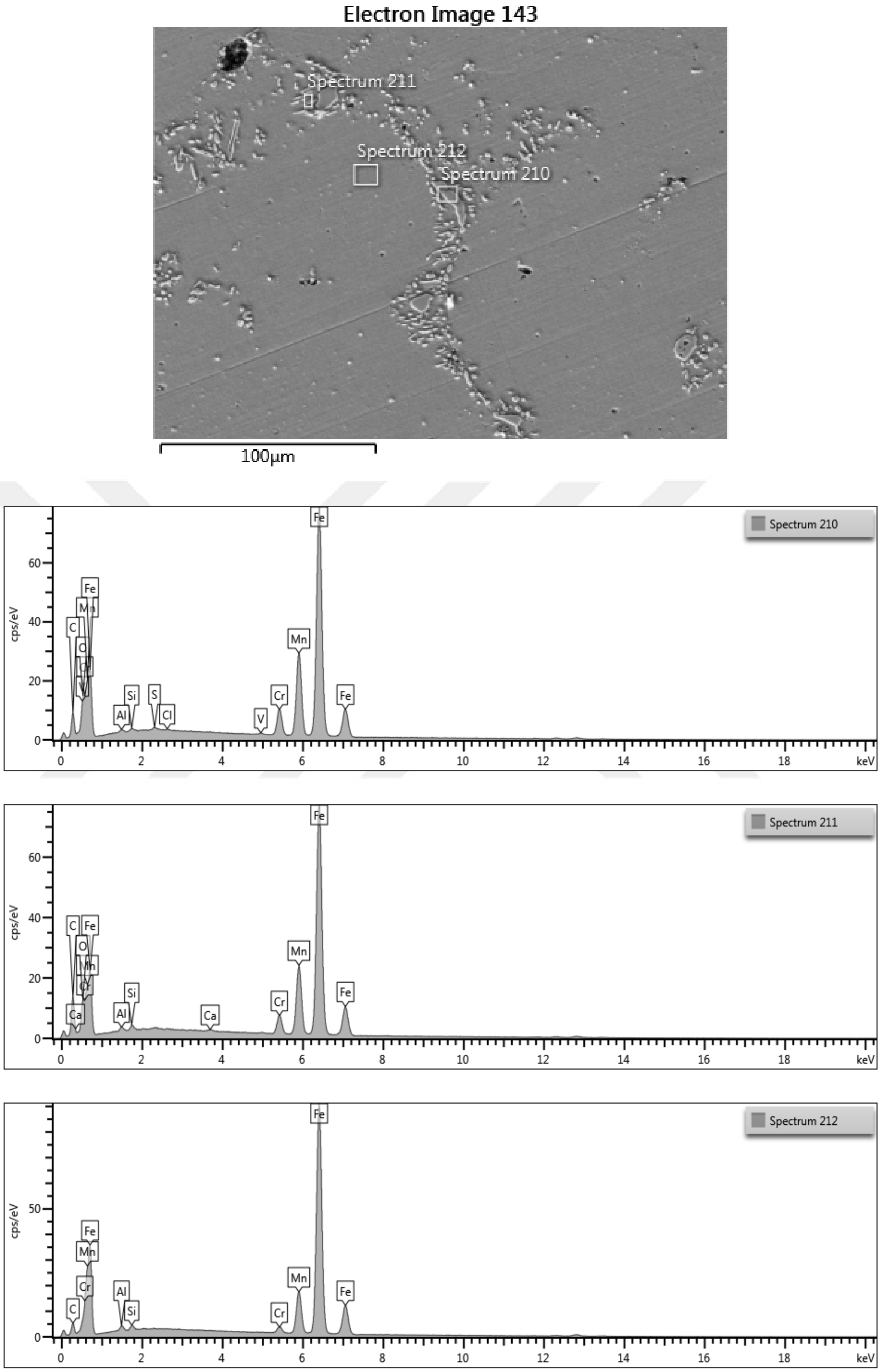

Figure 30: SEM-EDS images of GX120Mn13 material added 1% by weight of Al5Ti1B

Table 5: EDS values of GX120Mn13 material added 1% by weight of Al5Ti1B

Element	Spectrum 210		Spectrum 211		Spectrum 212	
	Wt%	Wt% Sigma	Wt%	Wt% Sigma	Wt%	Wt% Sigma
C	12.79	0.31	19.26	0.22	8.96	0.22
O	3.23	0.16	3.63	0.16		
Al	0.29	0.03	0.38	0.03	0.66	0.04
Si	0.23	0.03	0.39	0.03	0.52	0.03
S	0.14	0.03				
Cl	0.08	0.02				
Ca			0.13	0.02		
Cr	4.27	0.05	2.92	0.04	0.52	0.03
Mn	18.80	0.12	14.92	0.10	12.17	0.09
Fe	59.99	0.26	58.37	0.21	76.49	0.21
Total:	100		100		100	

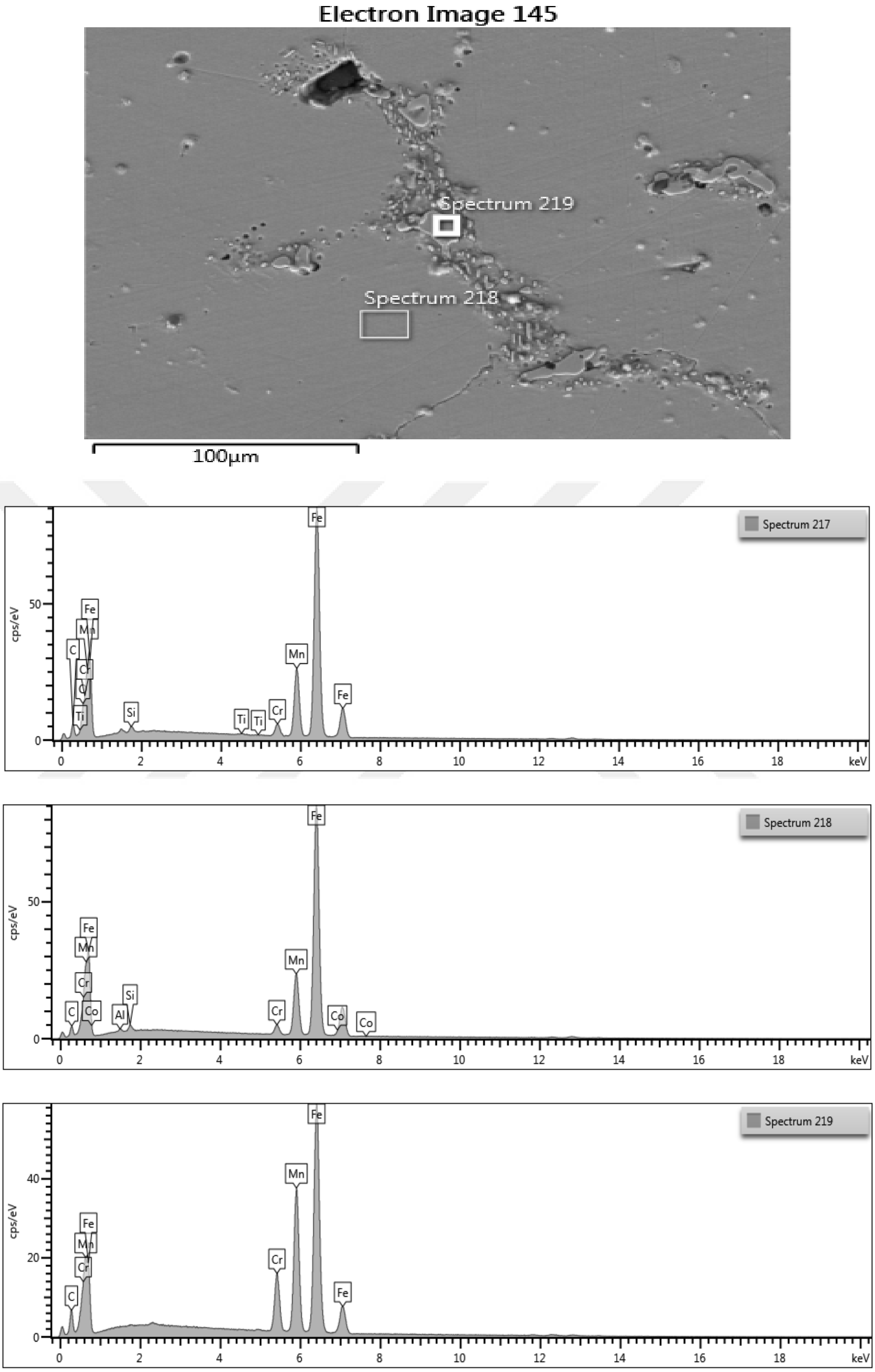

Figure 31: SEM-EDS images of GX120Mn17 material added 1% by weight of Al5Ti1B

Table 6: EDS values of GX120Mn17 material with 1% Al5Ti1B added by weight

Element	Spectrum 217		Spectrum 218		Spectrum 219	
	Wt%	Wt% Sigma	Wt%	Wt% Sigma	Wt%	Wt% Sigma
C	8.87	0.21	7.47	0.22	11.45	0.20
O	1.63	0.17				
Si	0.64	0.03	0.61	0.03		
Al			0.36	0.04		
Co			0.64	0.09		
Ti	0.10	0.03				
Cr	2.15	0.04	1.80	0.04	8.42	0.07
Mn	17.89	0.11	16.78	0.11	28.05	0.13
Fe	68.72	0.23	72.33	0.21	52.08	0.17
Total:	100		100		100	

4.3 Mechanical Properties

4.3.1 Vickers Hardness Measurement Results

Below are the Vickers hardness measurements and the mean, standard deviation of the measurement results. Maximum and minimum hardness values were measured as 272 HV and 231 HV in samples 7 and 3. It is usual to obtain higher hardness data in the hardness results in contact with the hard particles or to obtain different results in the hardness that contacts the porosity point, so it is seen that there are different hardness values. Addition of aluminum can dissolve carbides and $(Fe,Mn)_3AlC$ carbide formation can cause low hardness [25].

Table 7: Vickers hardness test results

Sample Number	VICKERS HARDNESS MEASUREMENT VALUES (HV)											
	1	2	3	4	5	6	7	8	9	10	Standard Deviation	Avarage
1	253.1	295.6	253.7	249	256.7	264.7	275.1	292	245.6	236	19.71402	262.15
2	316.1	239.5	256.7	271.8	246.7	255.5	248.4	233.6	243.9	308.8	28.56338	262.1
3	227.4	235.2	216.3	254.3	221.5	232	211.2	228.4	208.1	277.2	20.91842	231.16
4	262.8	244.5	277.2	217.7	246.7	269.2	234.1	227.4	232.6	224.9	20.15895	243.71
5	254.3	238.4	242.2	285.5	249	245.6	245.6	266.6	245.5	263.5	14.37929	253.62
6	234.1	254.3	256.7	268.6	262.2	273.8	280.6	277.2	251.3	268.6	14.05625	262.74
7	299.4	267.3	281.3	245.6	263.5	277.8	265.3	263.5	280.6	281.3	14.66911	272.56
8	249	240	238.4	266.6	251.9	242.8	262.2	247.9	262.2	254.9	9.81716	251.59
9	252.5	245.6	251.3	240.6	232.6	277.2	261.6	266	242.2	219.6	16.74036	248.92
10	246.7	259.7	233.1	242.8	230	230.5	256.71	228.41	246.1	256.1	12.00894	243.012

4.3.2 Abrasion Test Results

To obtain information about the friction coefficient behavior of GX120Mn13 and GX120Mn17 materials to which Al5Ti1B was added, friction coefficients were also measured during the wear tests and the graphs obtained are shown in the figures below. The related figures give the variation of the friction coefficient with the sliding distance of the materials under different loads. Although the coefficient of friction is not a determinant on its own, it often provides information about the wear behavior of materials. Since the friction force is coercive and in the opposite direction to the applied force, it causes the materials to wear out and complete their life. Therefore, a high coefficient of friction usually means low wear resistance.

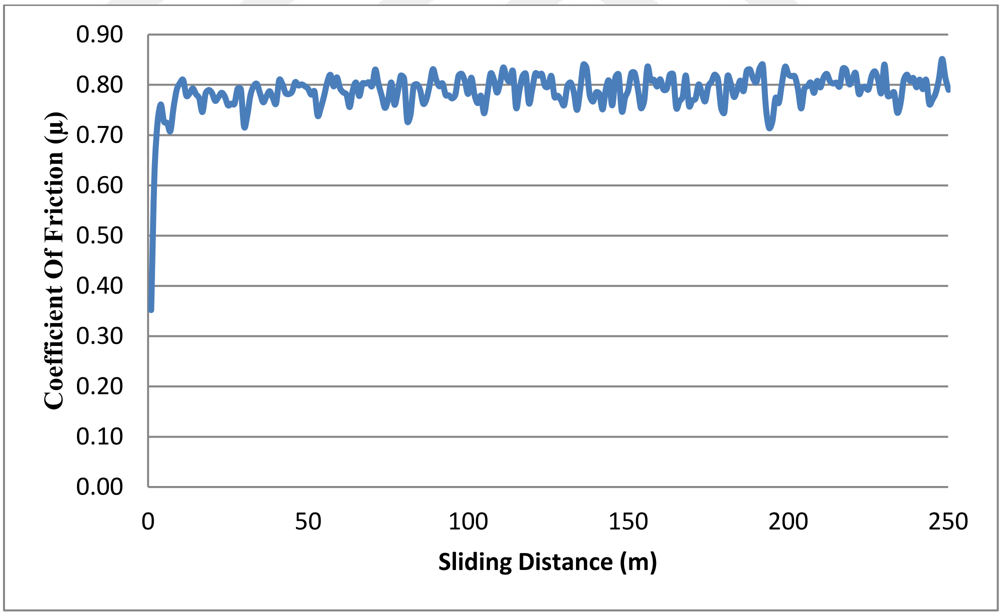

Figure 32: The friction coefficient-sliding distance relationship of GX120Mn13 material added 0.05% by weight of Al5Ti1B at 250 sliding distance under 5N load

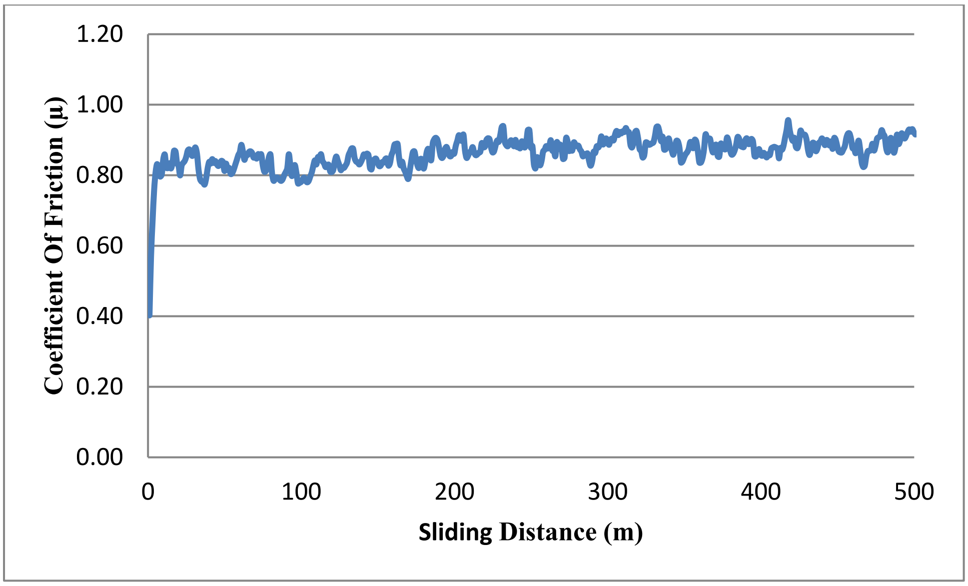

Figure 33: The friction coefficient-sliding distance relationship of GX120Mn13 material added 0.05% by weight of Al5Ti1B at 500 sliding distance under 5N load

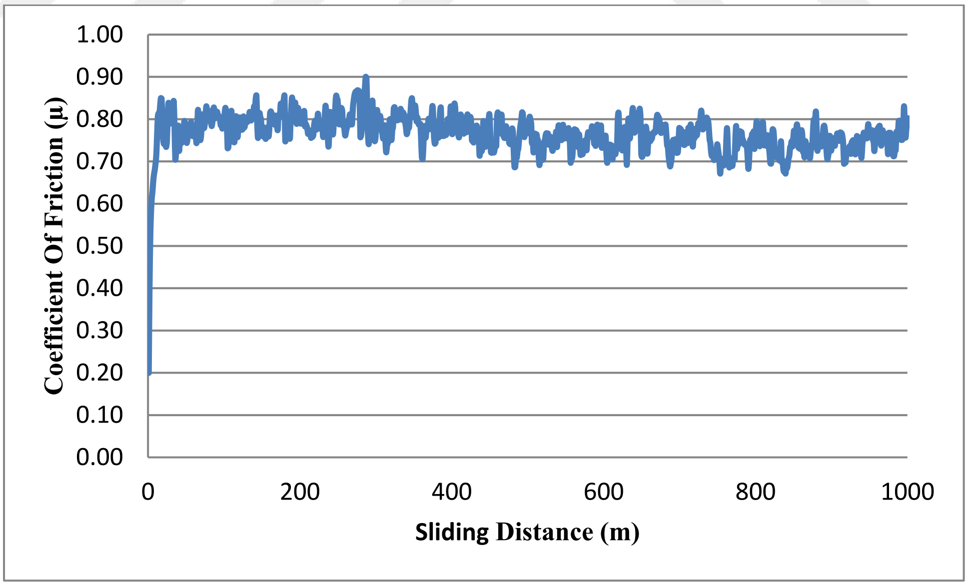

Figure 34: The friction coefficient-sliding distance relationship of GX120Mn13 material added 0.05% by weight of Al5Ti1B at 1000 sliding distance under 5N load

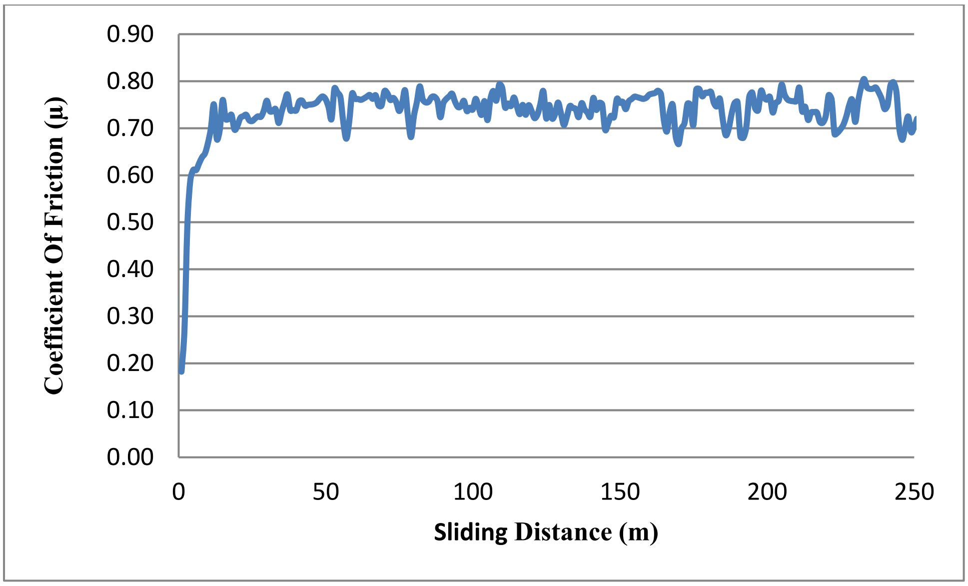

Figure 35: The friction coefficient-sliding distance relationship of GX120Mn13 material added 0.05% by weight of Al5Ti1B at 250 sliding distance under 10N load

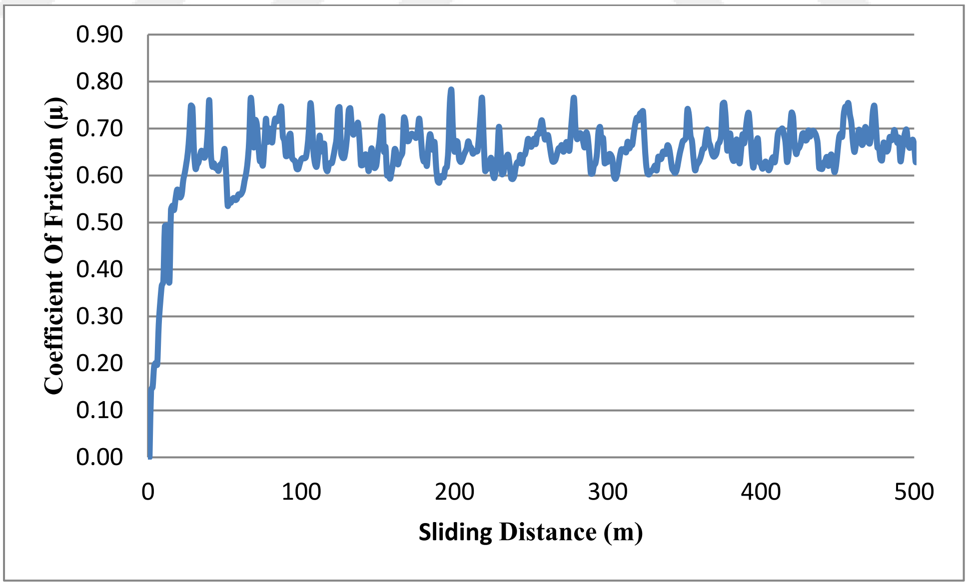

Figure 36: The friction coefficient-sliding distance relationship of GX120Mn13 material added 0.05% by weight of Al5Ti1B at 500 sliding distance under 10N load

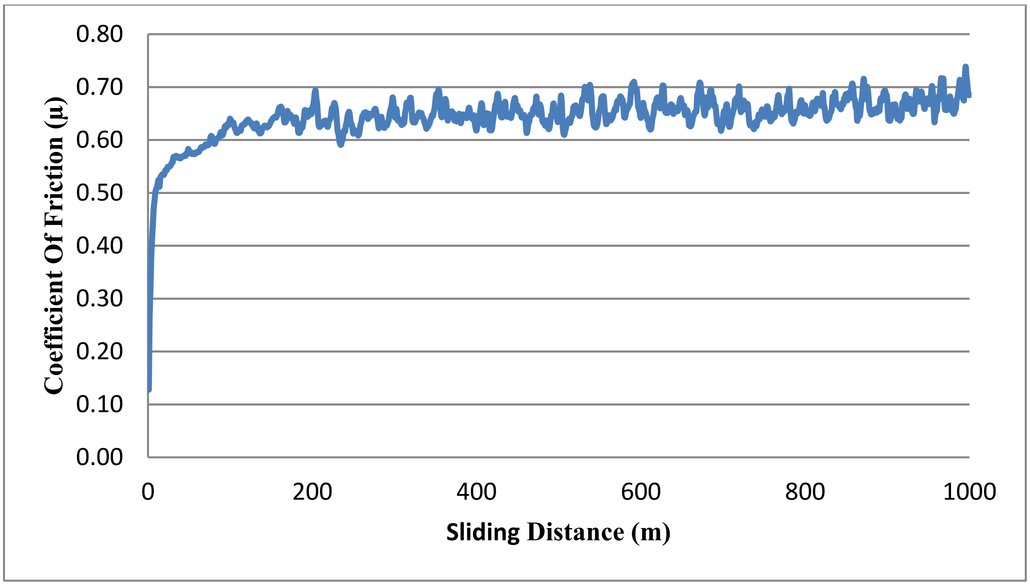

Figure 37: The friction coefficient-sliding distance relationship of GX120Mn13 material added 0.05% by weight of Al5Ti1B at 1000 sliding distance under 10N load

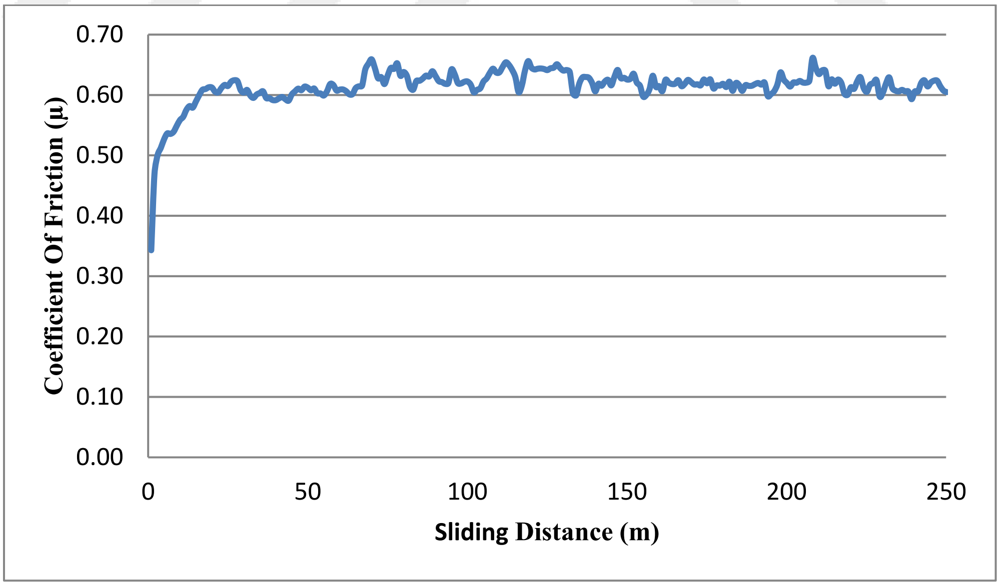

Figure 38: The friction coefficient-sliding distance relationship of GX120Mn13 material with 1% Al5Ti1B added by weight at 250 sliding distance under 5N load

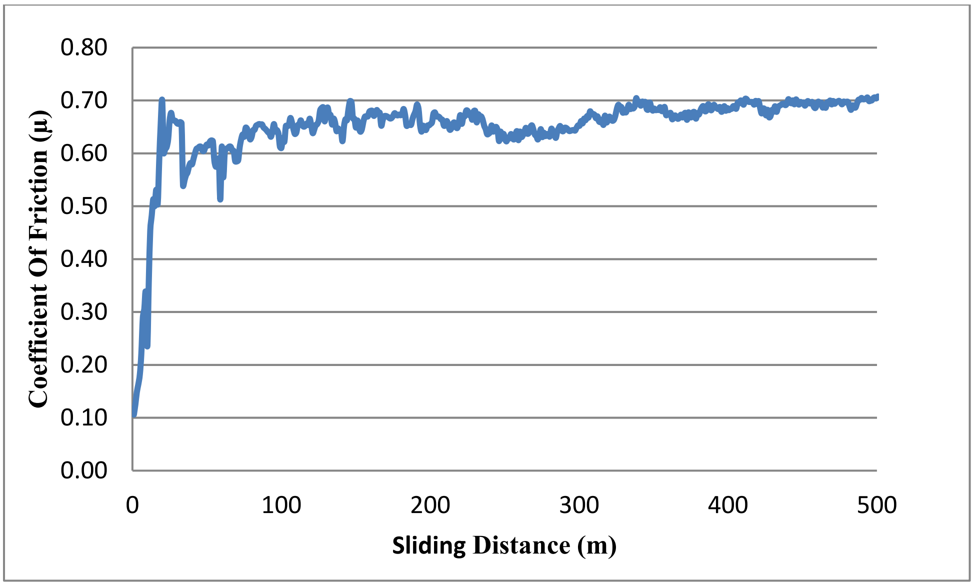

Figure 39: The friction coefficient-sliding distance relationship of GX120Mn13 material with 1% Al5Ti1B added by weight at 500 sliding distance under 5N load

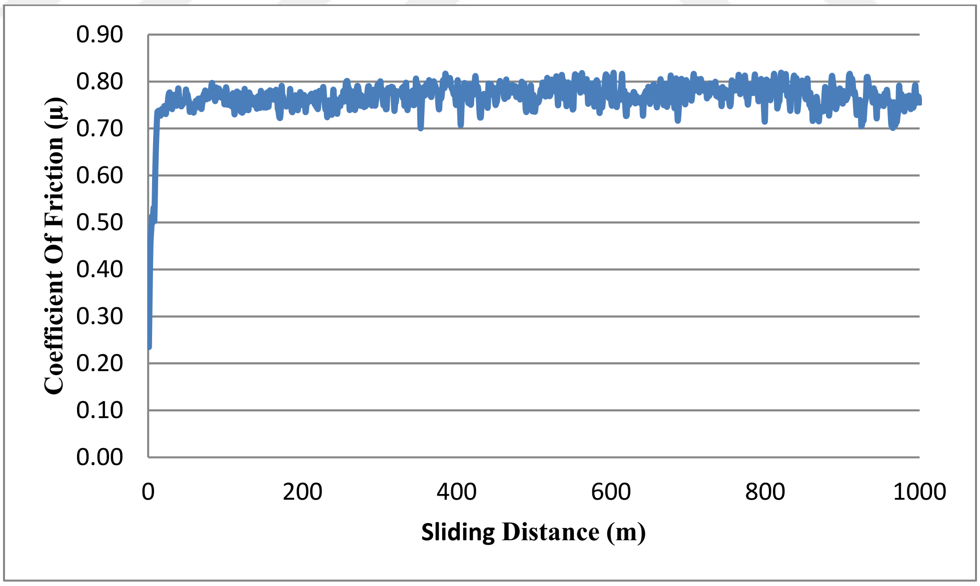

Figure 40: Friction coefficient-sliding distance relationship of GX120Mn13 material with 1% Al5Ti1B added by weight at 1000 sliding distance under 5N load

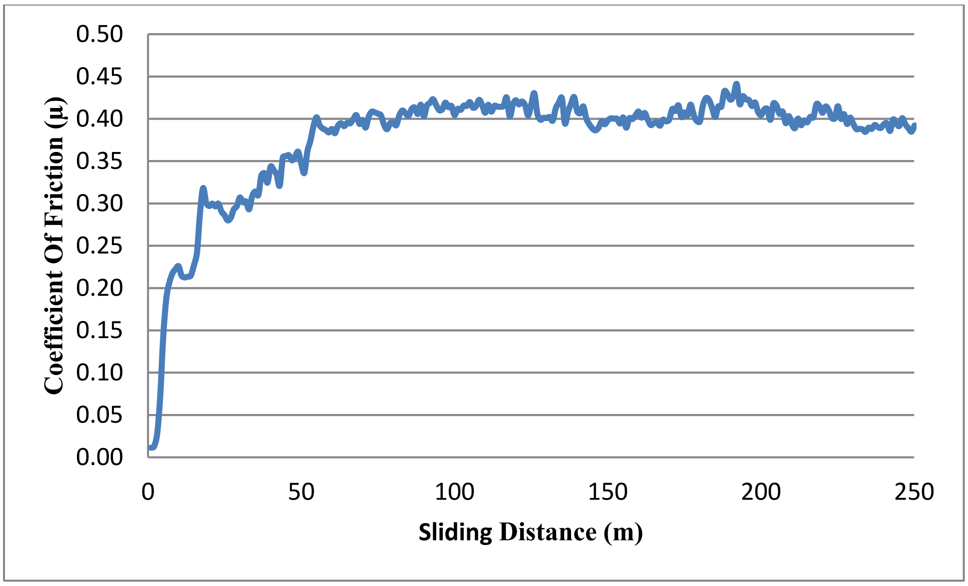

Figure 41: Friction coefficient-sliding distance relationship of GX120Mn13 material with 1% Al5Ti1B added by weight at 250 sliding distance under 10N load

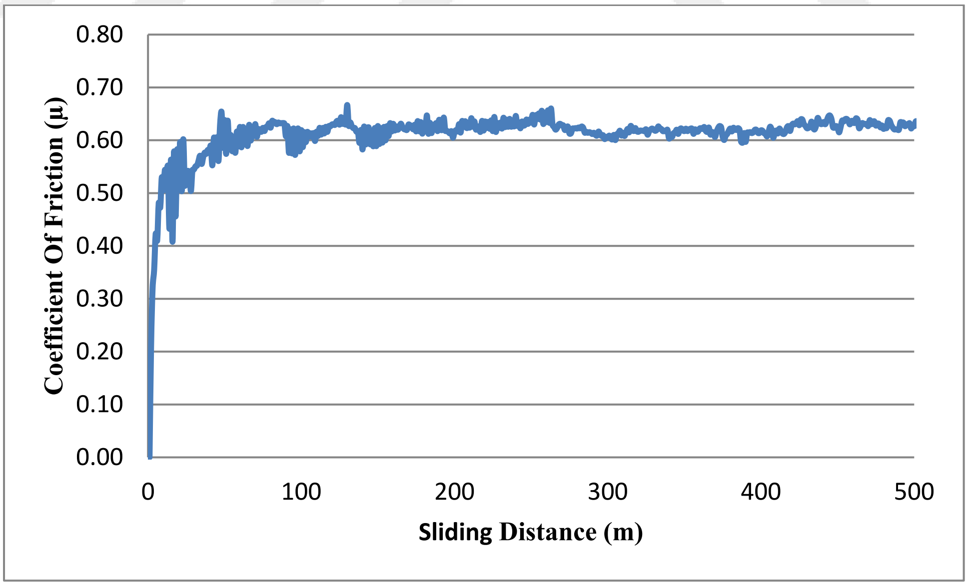

Figure 42: The friction coefficient-sliding distance relationship of GX120Mn13 material with 1% Al5Ti1B added by weight at 500 sliding distance under 10N load

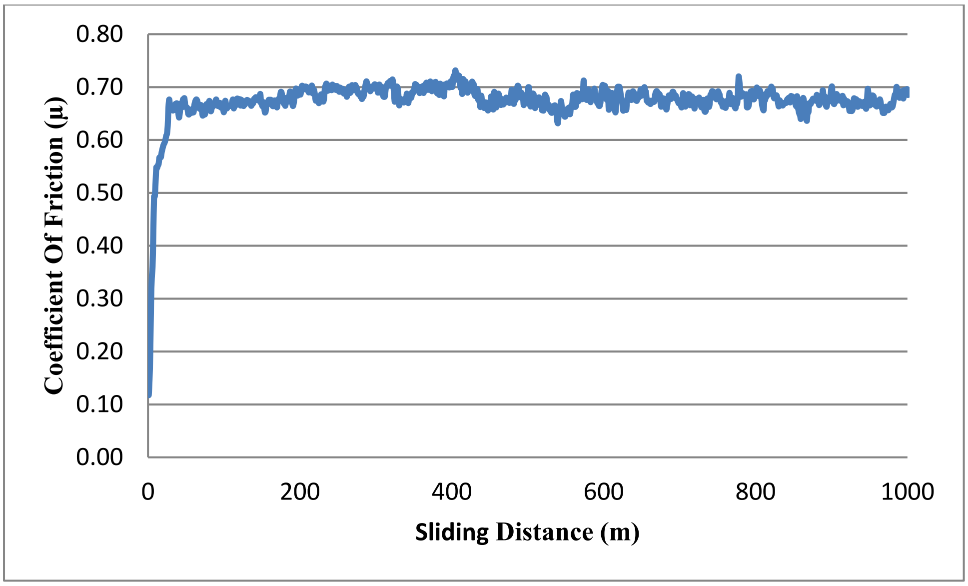

Figure 43: The friction coefficient-sliding distance relationship of GX120Mn13 material with 1% Al5Ti1B added by weight at 1000 sliding distance under 10N load

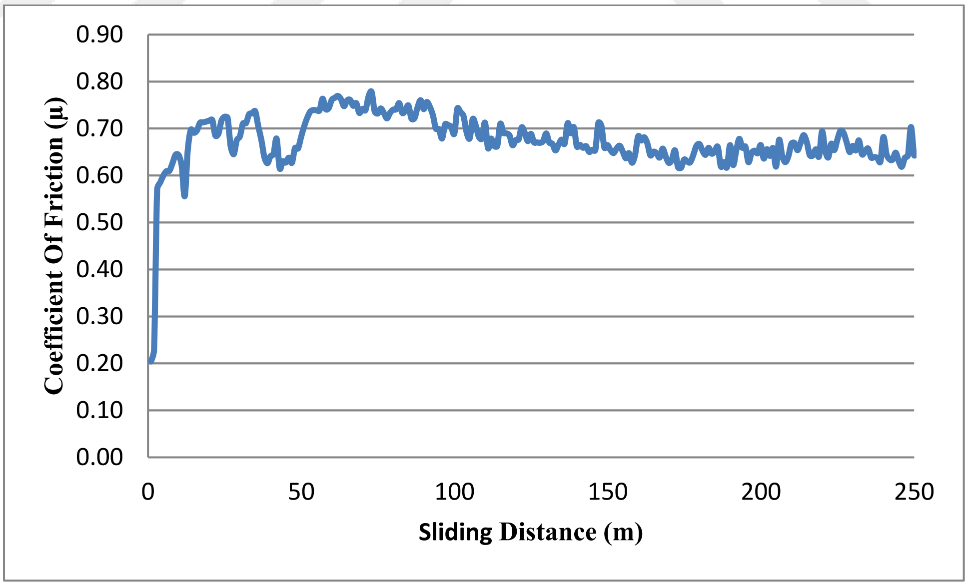

Figure 44: The friction coefficient-sliding distance relationship of GX120Mn17 material added 0.05% by weight of Al5Ti1B at 250 sliding distance under 5N load

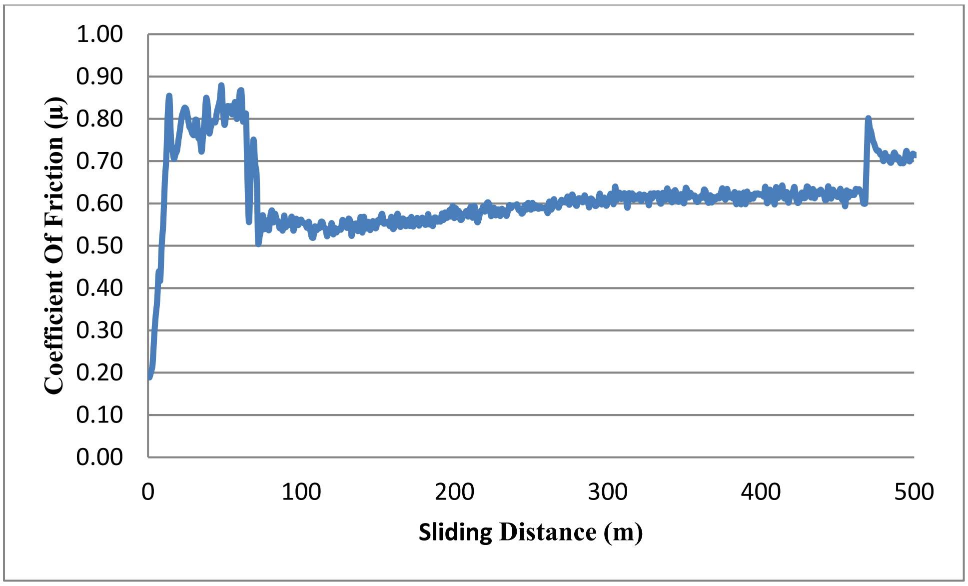

Figure 45: The friction coefficient-sliding distance relationship of GX120Mn17 material added 0.05% by weight of Al5Ti1B at 500 sliding distance under 5N load

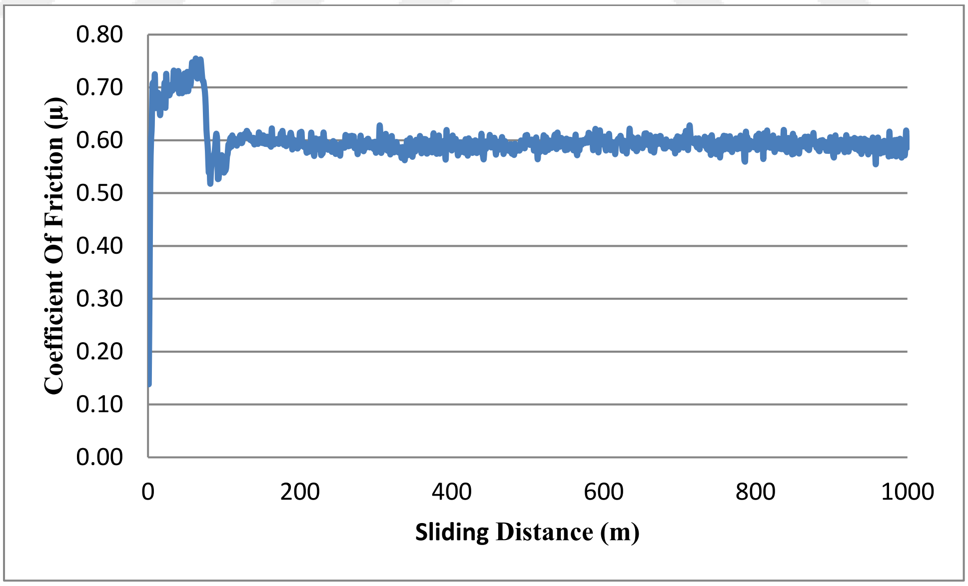

Figure 46: The friction coefficient-sliding distance relationship of GX120Mn17 material added 0.05% by weight of Al5Ti1B at 1000 sliding distance under 5N load

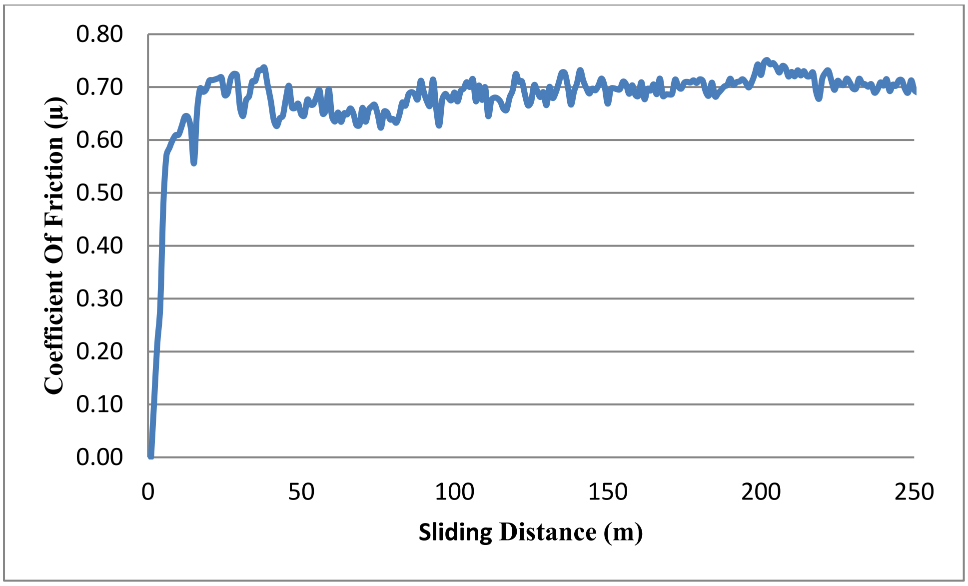

Figure 47: The friction coefficient-sliding distance relationship of GX120Mn17 material added 0.05% by weight of Al5Ti1B at 250 sliding distance under 10N load

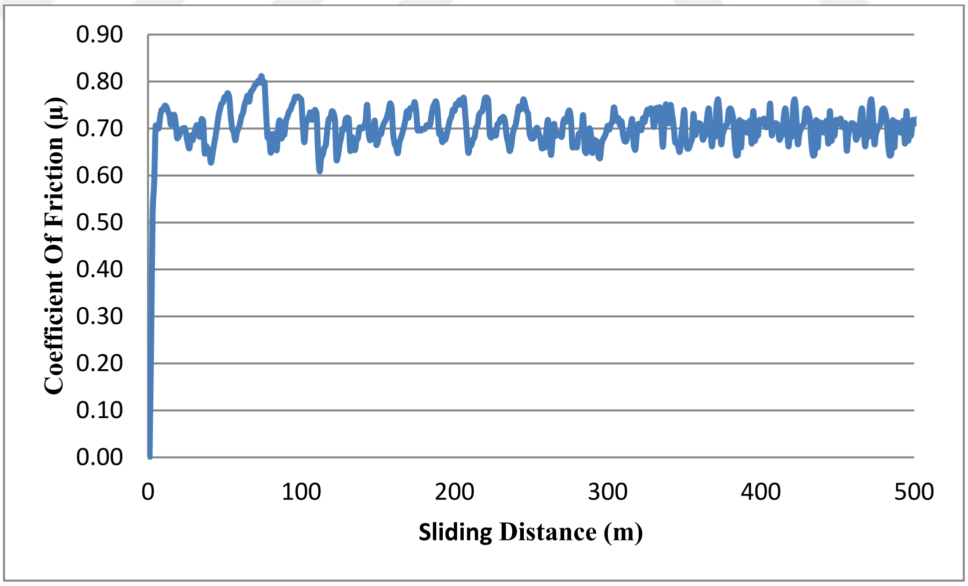

Figure 48: The friction coefficient-sliding distance relationship of GX120Mn17 material added 0.05% by weight of Al5Ti1B at 500 sliding distance under 10N load

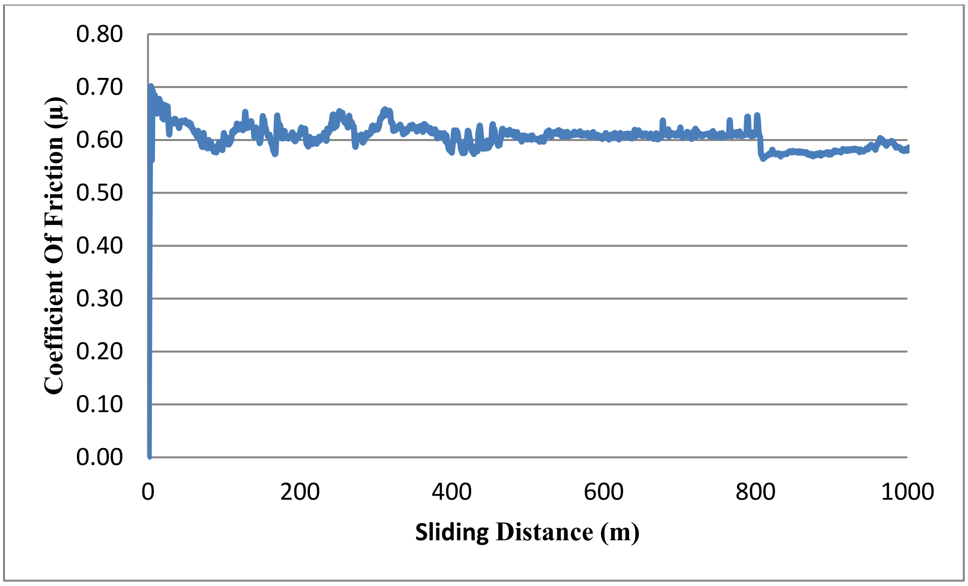

Figure 49: The friction coefficient-sliding distance relationship of GX120Mn17 material added 0.05% by weight of Al5Ti1B at 1000 sliding distance under 10N load

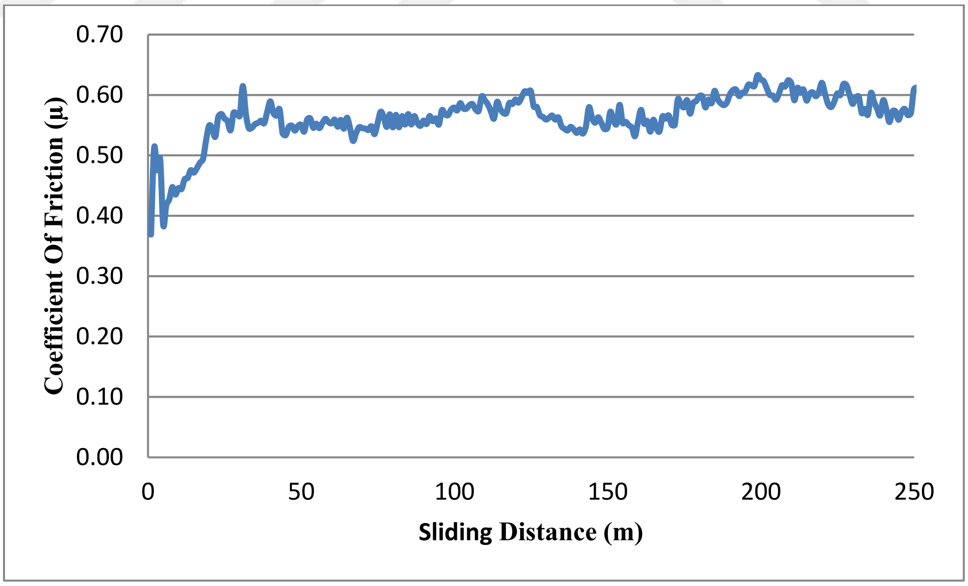

Figure 50: The friction coefficient-sliding distance relationship of GX120Mn17 material with 1% Al5Ti1B added by weight at 250 sliding distance under 5N load

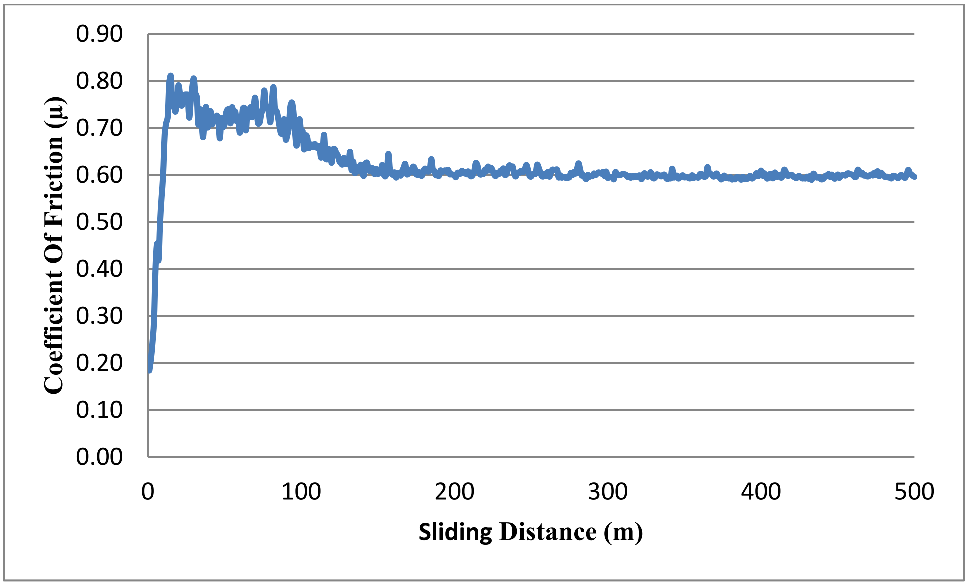

Figure 51: The friction coefficient-sliding distance relationship of GX120Mn17 material with 1% Al5Ti1B added by weight at 500 sliding distance under 5N load

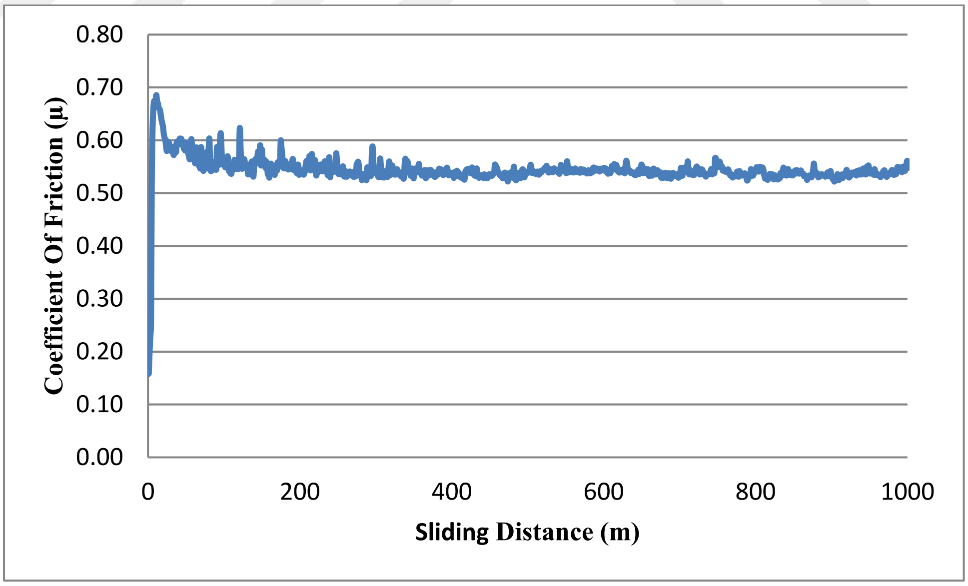

Figure 52: The friction coefficient-sliding distance relationship of GX120Mn17 material with 1% Al5Ti1B added by weight at 1000 sliding distance under 5N load

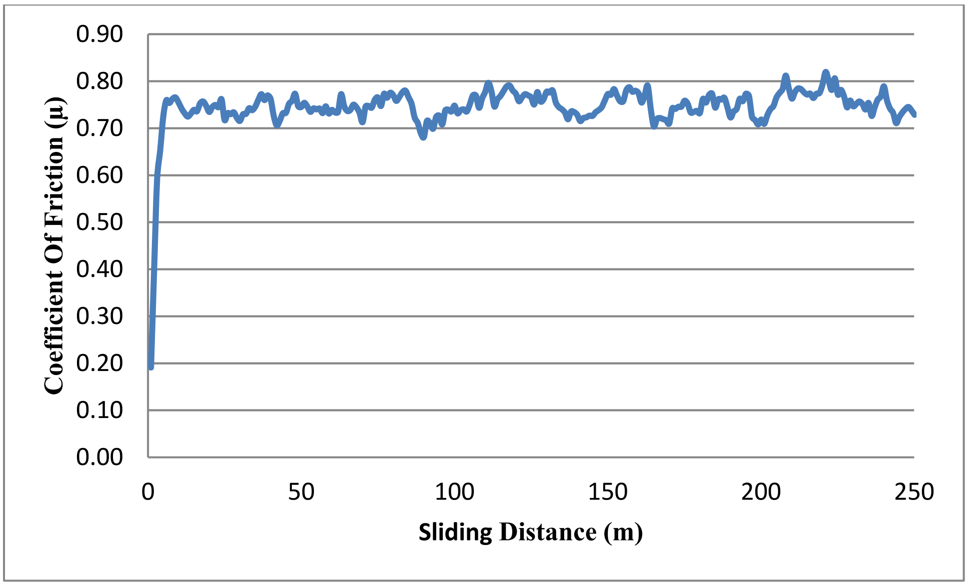

Figure 53: The friction coefficient-sliding distance relationship of GX120Mn17 material with 1% Al5Ti1B added by weight at 250 sliding distance under 10N load

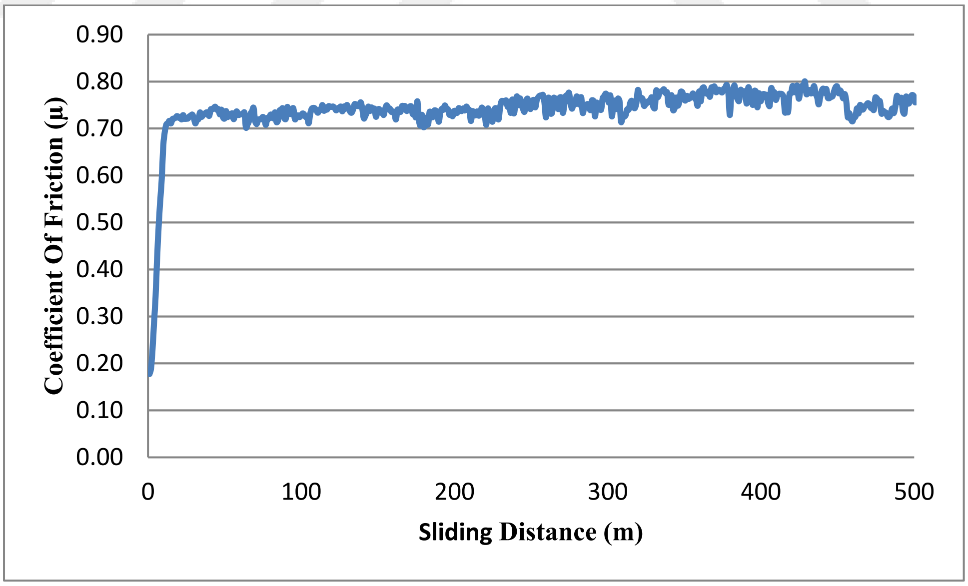

Figure 54: The friction coefficient-sliding distance relationship of GX120Mn17 material with 1% Al5Ti1B added by weight at 500 sliding distance under 10N load

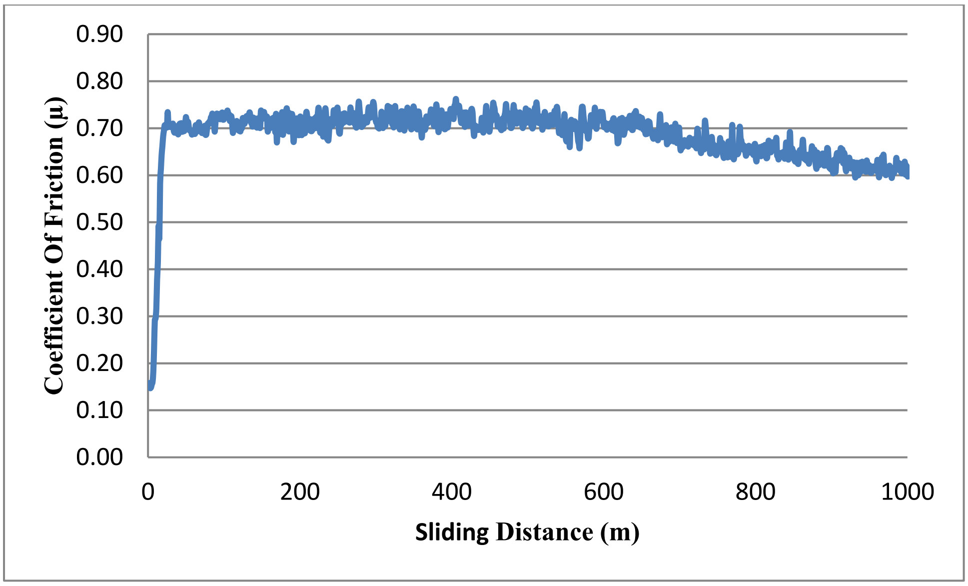

Figure 55: The friction coefficient-sliding distance relationship of GX120Mn17 material with 1% Al5Ti1B added by weight at 1000 sliding distance under 10N load

Initially, the friction coefficients for all samples have a rapid increase with sliding distance to an approximately constant range after about 50 m. This increase corresponds to an increase in the apparent contact area until full contact occurs across the full diameter of the pin. It has been observed that the friction coefficients of the materials increase in this sliding distance and then the friction coefficients are in a certain range. This range dilutes in the charts as a zigzag structure. The friction coefficient of GX120Mn17 material added 0.05% Al5Ti1B by weight at 500 and 1000 sliding distances under 5N load, and GX120Mn17 material with 1% Al5Ti1B added at 500 and 1000 sliding distances under 5N load significantly decreased after approximately 1000 m sliding distance and then zigzag was observed in its structure. This zigzag structure and unstable friction coefficients can be attributed to the changes in the microstructure of the materials and the hard phases formed. In Table 8, the variation of the average friction coefficient seen in the materials with the load and sliding distance is given.

Table 8: The variation of the average friction coefficient of Al5Ti1B added materials at different sliding distances under different loads.

Sample Code	Material	Load	Sliding Distance	Average Coefficient of Friction (μ)
1	GX120Mn13	5 N	250 m	0.7880
			500 m	0.8635
			1000 m	0.7656
		10 N	250 m	0.7361
			500 m	0.6471
			1000 m	0.6440
5		5 N	250 m	0.6142
			500 m	0.6500
			1000 m	0.7666
		10 N	250 m	0.3769
			500 m	0.6139
			1000 m	0.6739
6	GX120Mn17	5 N	250 m	0.6737
			500 m	0.6168
			1000 m	0.5990
		10 N	250 m	0.6816
			500 m	0.7037
			1000 m	0.6064
10		5 N	250 m	0.5637
			500 m	0.6236
			1000 m	0.5445
		10 N	250 m	0.7453
			500 m	0.7407
			1000 m	0.6836

The average coefficient of friction was observed with a maximum value of 0.8635 in GX120Mn13 material under 5N load and 500 m sliding distance. The minimum average friction coefficient was obtained with a value of 0.3769 in GX120Mn13 material under 10 N load and 250 m sliding distance. These changes depend on the hardness value of the materials and the formation of hard particles. The particles support the load to reduce the contact area between the pin and the counter disc surface, reduce the friction coefficient, and prevent scratching and cutting from the surface [26]. In addition, it is seen that the average friction coefficient decreases at the same sliding distances with the increase in load for GX120Mn13 materials. However, in GX120Mn17 materials, it was determined that the average friction coefficient increased with the increase in load at the same sliding distances. Different materials exhibited different characteristics. In Figures 56, 57, 58, 59, weight losses of GX120Mn13 and GX120Mn17 materials with added 0.05% and 1% Al-5TiB by weight are given at different shear rates under 5 N and 10 N loads. It is clearly seen that the wear losses increase with the sliding distance of the materials and the applied load. In Table 9, the wear volume loss and wear rate values of the materials are given. Maximum wear volume loss and wear rate were obtained in GX120Mn13 material under 10N load and 1000 m sliding distance. Minimum wear volume loss was obtained in GX120Mn13 material under 5 N load and 250 m sliding distance. The addition of Al5Ti1B to the GX120Mn13 material did not reduce the wear loss, but the wear loss was significantly reduced in the GX120Mn17 material.

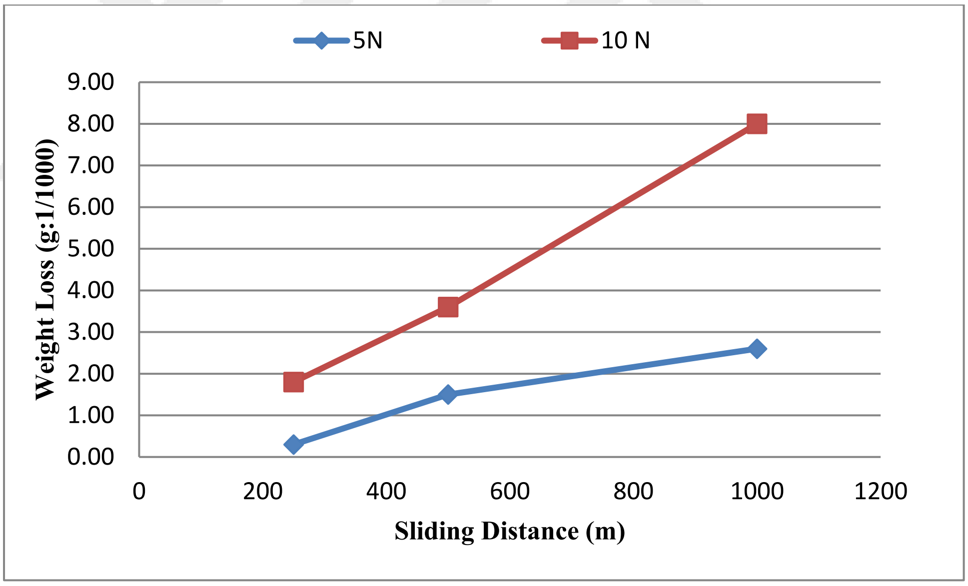

Figure 56: Variation of weight loss with sliding distance of GX120Mn13 material added 0.05% Al5Ti1B by weight

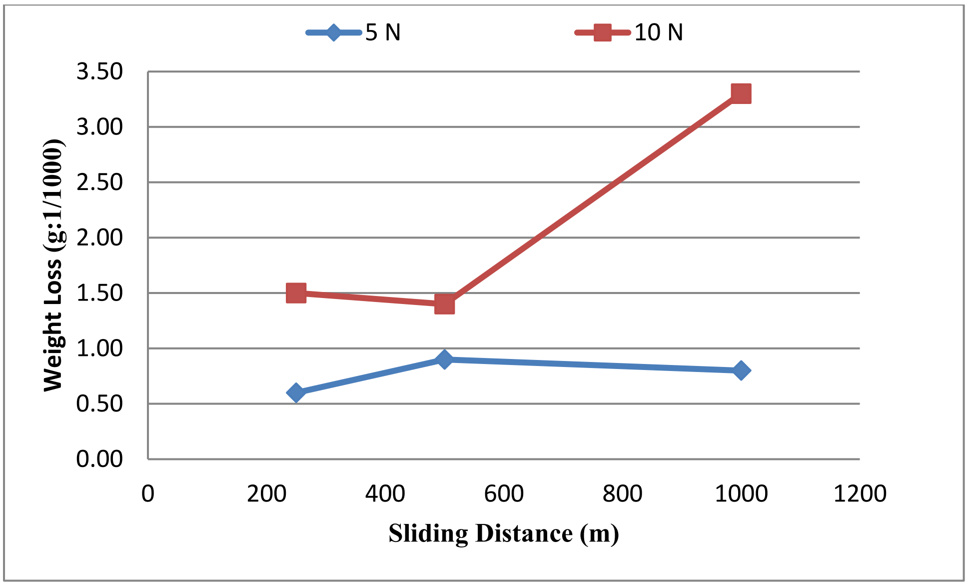

Figure 57: Variation of weight loss with sliding distance of GX120Mn13 material added 1% by weight of Al5Ti1B

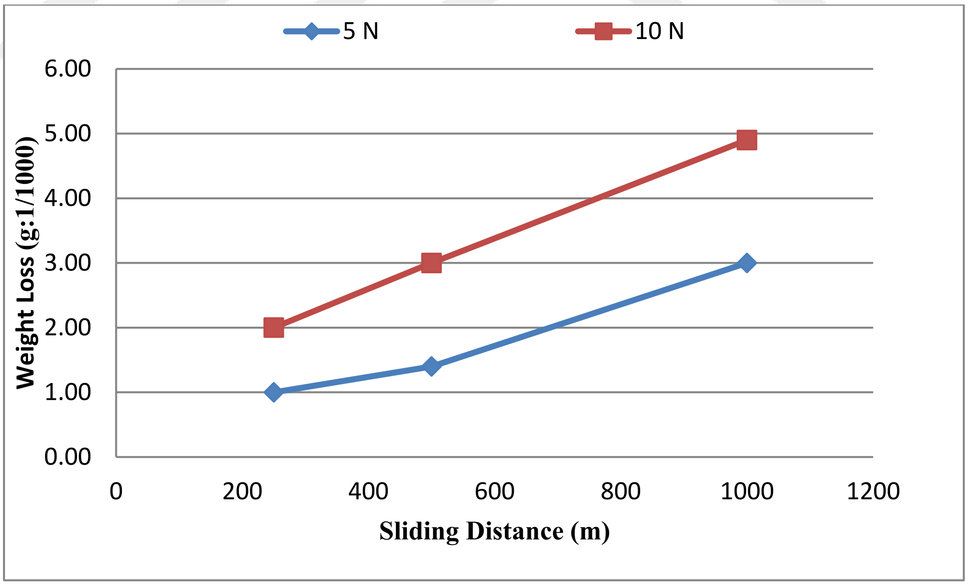

Figure 58: Variation of weight loss with sliding distance of GX120Mn17 material added 0.05% Al5Ti1B by weight

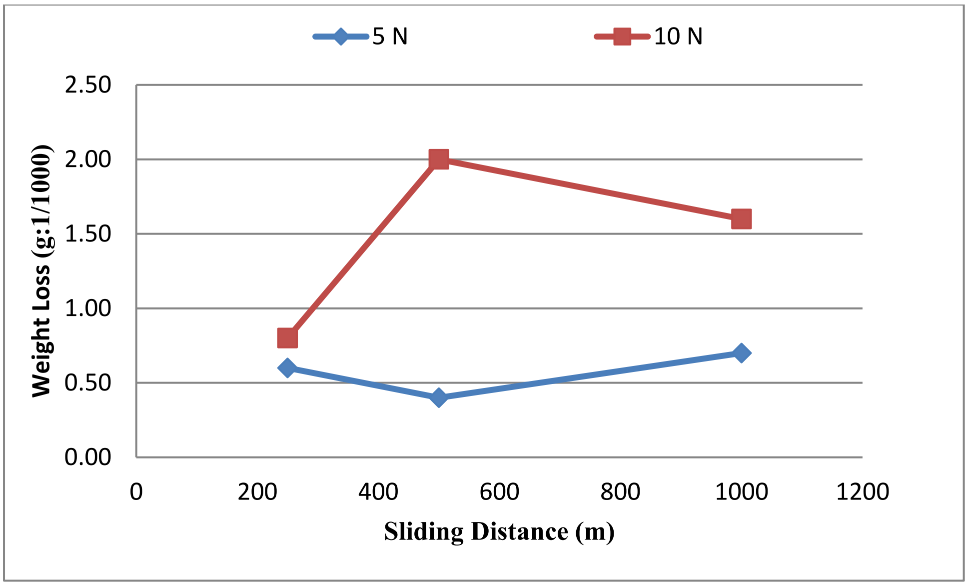

Figure 59: Variation of weight loss with sliding distance of GX120Mn17 material added 1% by weight of Al5Ti1B

Table 9: Abrasion Volume Loss and Abrasion Rates of Al5Ti1B added materials at different sliding distances under different loads

Sample Code	Material	Load	Sliding Distance	Abrasion Loss of Volume (mm^3)	Wear Rate (mm^3/km)
1	GX120Mn13	5 N	250 m	0.038973946	0.155895784
1	GX120Mn13	5 N	500 m	0.194869730	0.389739459
1	GX120Mn13	5 N	1000 m	0.337774198	0.337774198
1	GX120Mn13	10 N	250 m	0.233843676	0.935374702
1	GX120Mn13	10 N	500 m	0.467687351	0.935374702
1	GX120Mn13	10 N	1000 m	1.039305224	1.039305224
5	GX120Mn13	5 N	250 m	0.078441626	0.313766505
5	GX120Mn13	5 N	500 m	0.117662440	0.235324879
5	GX120Mn13	5 N	1000 m	0.104588835	0.104588835
5	GX120Mn13	10 N	250 m	0.196104066	0.392208132
5	GX120Mn13	10 N	500 m	0.183030461	0.183030461
5	GX120Mn13	10 N	1000 m	0.431428945	0.431428945
6	GX120Mn17	5 N	250 m	0.129913153	0.519652612
6	GX120Mn17	5 N	500 m	0.181878414	0.363756829
6	GX120Mn17	5 N	1000 m	0.389739459	0.389739459
6	GX120Mn17	10 N	250 m	0.259826306	1.039305224
6	GX120Mn17	10 N	500 m	0.389739459	0.779478918
6	GX120Mn17	10 N	1000 m	0.636574450	0.636574450
10	GX120Mn17	5 N	250 m	0.078441626	0.313766505
10	GX120Mn17	5 N	500 m	0.052294418	0.104588835
10	GX120Mn17	5 N	1000 m	0.091515231	0.091515231
10	GX120Mn17	10 N	250 m	0.104588835	0.418355341
10	GX120Mn17	10 N	500 m	0.261472088	0.522944176
10	GX120Mn17	10 N	1000 m	0.209177670	0.209177670

As expected, the weight loss and wear rate values for samples under an applied load of 10 N are greater for a 5 N load. It can be explained by the separation of the surface roughness at higher load and therefore the increase in the number of contact roughnesses and consequently the increase in the worn surface material. As a general rule of wear, increasing the hardness of the material increases the wear resistance. However, if the material becomes brittle at the end of this hardness increase, wear resistance at high loads may be adversely affected. It is thought that the secondary phases and particles precipitated in the structure by the addition of boron and titanium during wear at high loads break off from the structure at high loads and increase the weight loss. These changes are also consistent with the hardness results. According to Archard's law, the higher the hardness of a material, the less wear loss on the surface and the higher the wear resistance is expected. However, as a result of the deformation and hardening that may occur in the materials, the substrate material showed higher resistance to the abrasive ball, resulting in an increase in wear rates. It is thought that this causes a decrease in wear volume losses [27, 28].

4.3.3 Wear Surface SEM Results

According to the wear test results, scanning electron microscope images of the wear surfaces of the samples are given in the figures below. Scanned electron images of wear surfaces selected from samples showing minimum and maximum wear volume loss are given. It is seen that the amount of deformation on the wear surface increases with increasing load. It is clearly seen that there are ruptures and ruptures on the material surface as a result of wear. In the wear tests carried out, the wear mechanism consists of surface scratches and cavities. Due to the repeated plastic deformation with increasing load, the depth of surface scratches and surface cavities increase along with the amount and depth of some materials. Due to the denser formation of carbides in GX120Mn17 material, wear occurs more in the matrix and it is seen that the material is more resistant to wear.

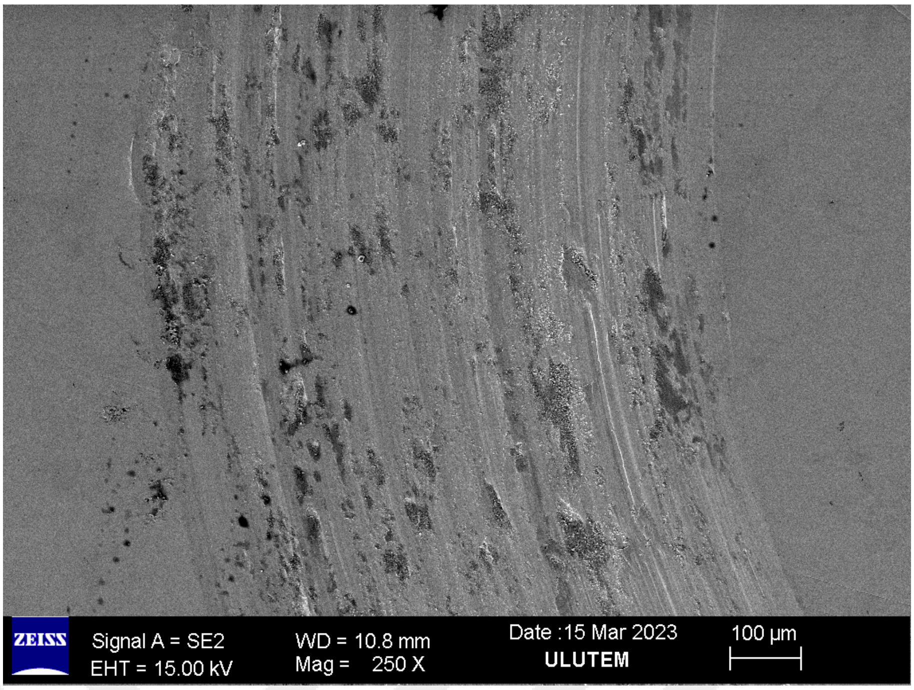

Figure 60: Scanning electron microscope image of wear surface of GX120Mn13 material with 0.05% Al5Ti1B added by weight at 250 m sliding distance under 5 N load.

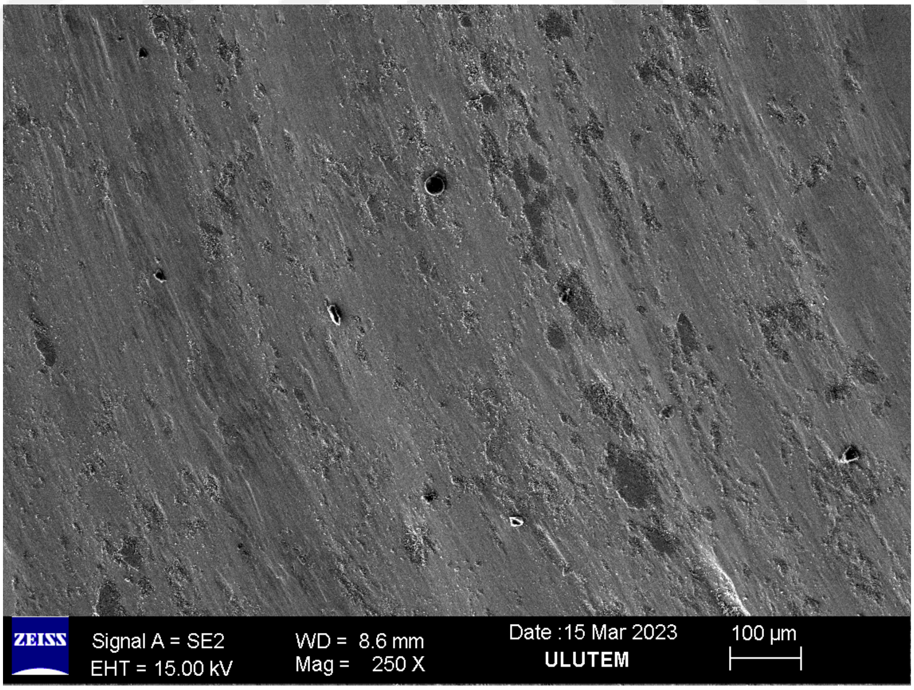

Figure 61: Scanning electron microscope image of wear surface of GX120Mn13 material with 0.05% Al5Ti1B added by weight at 1000 m sliding distance under 10 N load

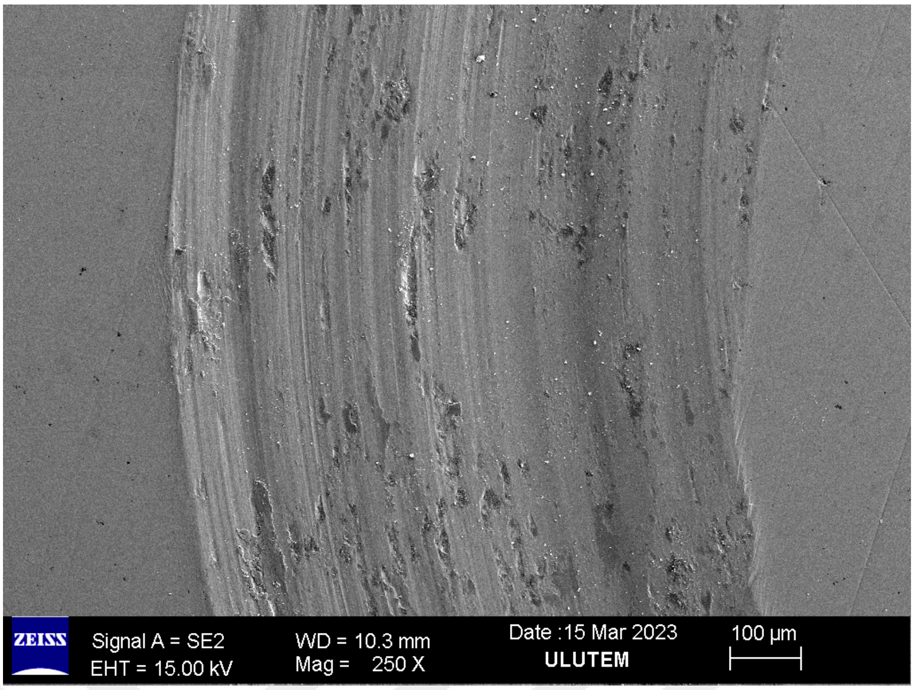

Figure 62: Scanning electron microscope image of wear surface of GX120Mn13 material with 1% Al5Ti1B added by weight at 250 m sliding distance under 5 N load.

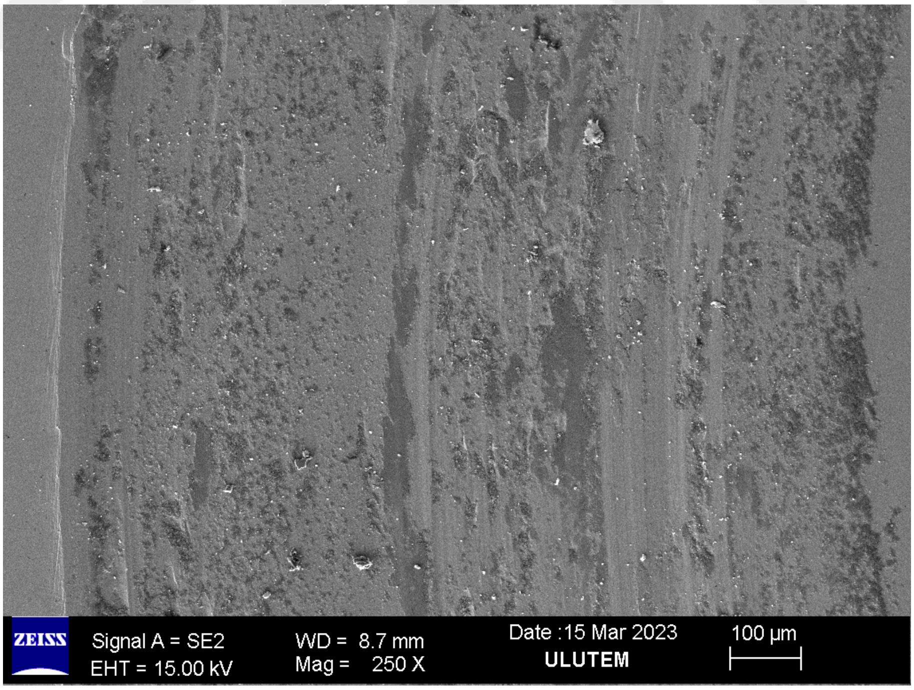

Figure 63: Scanning electron microscope image of wear surface of GX120Mn13 material with 1% Al5Ti1B added by weight at 1000 m sliding distance under 10 N load

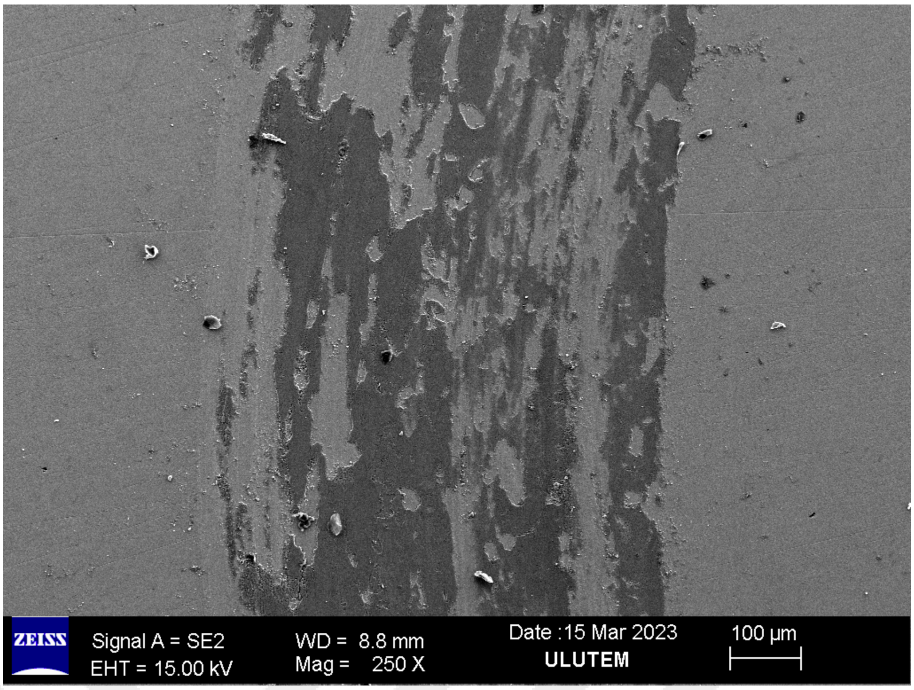

Figure 64: Scanning electron microscope image of the wear surface of the GX120Mn17 material with 0.05% Al5Ti1B added by weight at a sliding distance of 250 m under 5 N load.

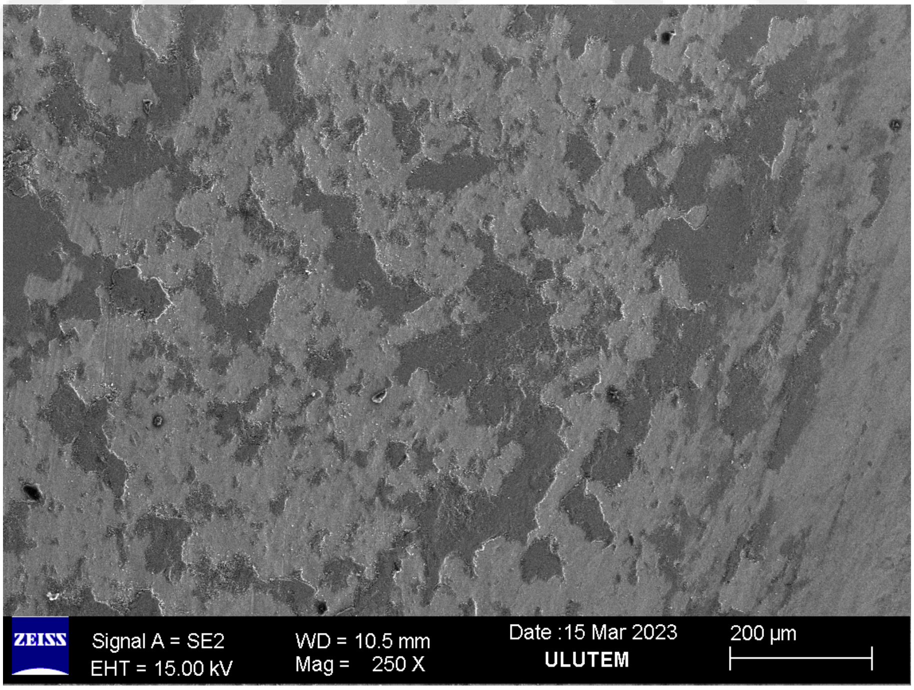

Figure 65: Scanning electron microscope image of wear surface of GX120Mn17 material with 0.05% Al5Ti1B added by weight at 1000 m sliding distance under 10 N load

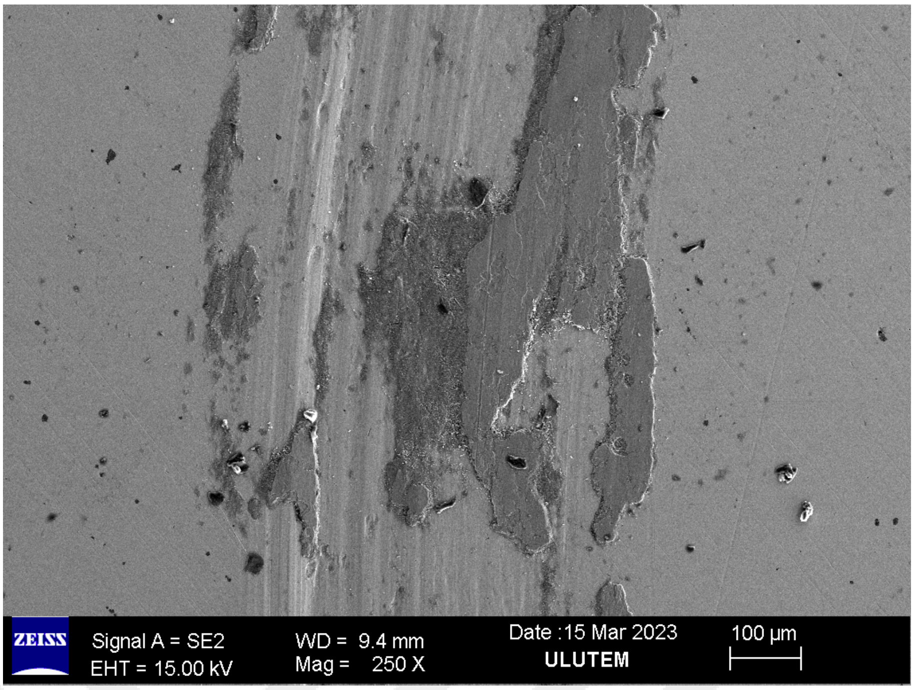

Figure 66: Scanning electron microscope image of wear surface of GX120Mn17 material with 1% Al5Ti1B added by weight at 500 m sliding distance under 5 N load.

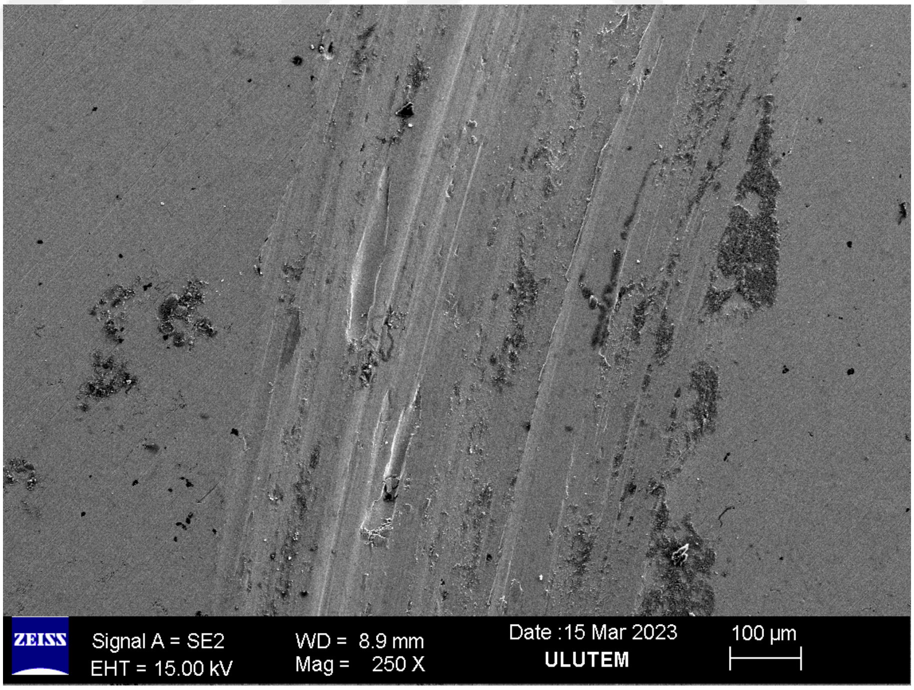

Figure 67: Scanning electron microscope image of wear surface of GX120Mn17 material with 1% Al5Ti1B added by weight at 500 m sliding distance under 10 N load.

CHAPTER 5
CONCLUSION

In today's engineering studies, it is of great importance to develop the properties of the materials used to meet the important needs of technology. In this sense, austenitic manganese steels have very wide and critical usage areas. In this study, it was aimed to investigate the optimum microstructure and mechanical properties by examining the effect of Al5Ti1B master alloy on the microstructure and mechanical properties of high Mn austenitic steel casting samples with different Mn ratios produced by sand casting method.

Al5Ti1B was added as 0.05%, 0.1%, 0.2%, 0.5% and 1% by weight, respectively, to the GX120Mn13 and GX120Mn17 material melted in the induction furnace and the melt was poured into the prepared sand mold. The microstructures of the produced materials were investigated by means of optical and scanning electron microscopy, and their mechanical properties were investigated by carrying out hardness and wear tests. In addition, compositions were made by spectral analysis and electron distribution spectrum, and wear surfaces were examined by scanning electron microscopy. The obtained results can be summarized as follows.

• The presence of master alloys added to the materials was confirmed by spectral analysis.
• Grain boundary carbides were detected with the austenitic matrix of the samples.
• Samples showed austenitic and pertilitic matrix formation.
• It has been observed that the carbides in the cast structure affect the hardness of the samples.
• Maximum hardness in GX120Mn13 material was obtained by adding 0,05% Al5Ti1B and in GX120Mn17 material with the addition of 0.2% Al5Ti1B.
• Average coefficient of friction values varied according to the matrix used, load change, sliding distance and added master alloy.

• It has been observed that the wear volume ratios increase with sliding distance and increasing load.

• The improvement in wear is attributed to increasing strain hardening and hardness change.

REFERENCES

[1] KAYADELEN A., (2018) "Yüksek Manganlı Ostenitik Çeliklerin Aşınma Davranışlarına Vanadyum ve Molibden Element İlavesinin Etkisinin İncelenmesi'', Eskişehir Osmangazi Üniversitesi, Fen Bilimleri Enstitüsü, Yüksek Lisans Tezi, Eskişehir

[2] GÜROL U., (2020) "Döküm Proses Parametrelerinin Yüksek Manganlı Östenitik Çeliklerin Özelliklerine Etkisinin İncelenmesi", Sakarya Üniversitesi, Fen Bilimleri Enstitüsü, Doktora Tezi, Sakarya

[3] MAHLAMI C.S., PAN X., (2014) "An Overview On High Manganese Steel Casting'', University of Johannesburg, Johannesburg, South Africa

[4] SUTTON, B. J., (2013) "Solidification Behavior and Hot Cracking Susceptibility of High Manganese Steel Weld Metals", The Ohio State University

[5] TUTAR, M., (2017) "Kaynaklı Twip Çeliklerinde Mikroyapı Ve Mekanik Özellikler Arasındaki İlişkilerin Araştırılması", Uludağ Üniversitesi, Doktora Tezi, Bursa

[6] CORNETTE D., CUGY P., HİLDENBRAND A., BOUZEKRİ M., (2005) "Ultra High Strength FeMn TWIP Steels for Automotive Safety Parts", 2005 SAE World Congress, Detroit, Michigan

[7] AYTEKİN, V., "Yüksek Manganezli Östenitik Çeliklerin Metallürjik Özellikleri", Orta Doğu Teknik Üniversitesi, Ankara

[8] MOUSAVİ ANİJDAN S. H., SABZI M., (2018) "The Effect Of Heat Treatment Process Parameters On Mechanical Properties, Precipitation, Fatigue Life, And Fracture Mode Of An Austenitic Mn Hadfield Steel", Journal of Materials Engineering and Performance

[9] AZADI M., PAZUKİ A. M., OLYA M. J.; (2018) "The Effect of New Double Solution Heat Treatment on the High Manganese Hadfield Steel Properties'', Springer Science+Business Media, LLC, part of Springer Nature and ASM International

[10] DASTUR Y. N., LESLIE W. C.; (1981) "Mechanism of Work Hardening in Hadfield Manganese Steel'', Amerıcan Socıety For Metals And The Metallurgıcal Socıety Of Aime

[11] ZUIDEMA B. K., SUBRAMANYAM D. K., LESLIE W. C., (1987) "The Effect Of Aluminum On The Work Hardening And Wear Resistance Of Hadfield Manganese Steel", University of Michigan

[12] KUMAR, D., (2015) "Design Of High Manganese Steels: Calculation Of SFE And MS Temperature", Department Of Metallurgical And Materials Engineering, Indian Institute Of Technology, West Bengal, India

[13] PIERCE D. T., JIMENEZ J. A., BENTLEY J., RAABE D., OSKAY C., WITTING J. E.; (2014) "The İnfluence Of Manganese Content On The Stacking Fault And Austenite/E-Martensite İnterfacial Energies İn Fe–Mn–(Al–Si) Steels İnvestigated By Experiment And Theory'', Vanderbilt University, Dusseldorf, Germany

[14] VENTURELLI B. N., ALBERTIN E., ROBERTO E., AZEVEDO F.; "The Effect Of The Austenite Grain Refinement On The Tensile And İmpact Properties Of Cast Hadfield Steel'', Escola Politecnica University, Sao Paulo, Brazil

[15] MAHLAMI C. S., PAN X., (2014) "Mechanical Properties And Microstructure Evaluation Of High Manganese Steel Alloyed With Vanadium'', University Of Johannesburg, Department Of Metallurgy, South Africa

[16] BERME B.; (2011) "Effects Of Strain Rates On The Mechanical Properties Of High Manganese Austenitic Steels'', İstanbul Teknik Üniversitesi, Fen Bilimleri Enstitüsü, Yüksek Lisans Tezi, İstanbul,

[17] ERDEM S.; (2006) "Yüksek Karbon İçeriğine Sahip, Yüksek Kromlu, Manganlı Ve Alaşımsız Düşük Karbonlu Çeliklerin Aşınma Davranışlarının

Araştırılması'', Fırat Üniversitesi, Fen Bilimleri Enstitüsü, Yüksek Lisans Tezi, Elazığ

[18] TURHAN H.; (1994) "Östenitik Manganlı Çeliğin Aşınma Davranışlarının Araştırılması'', Fırat Üniversitesi, Fen Bilimleri Enstitüsü, Yüksek Lisans Tezi, Elazığ

[19] SEZGİN C. T,; (2022) "Nitrasyon Ve Borlama Yapılan Yüksek Manganlı Çeliğin Korozif Ve Aşınma Özelliklerinin İncelenmesi'', Karabük Üniversitesi, Fen Bilimleri Enstitüsü, Doktora Tezi, Karabük

[20] SABZI M., FARZAM M.; (2019) "Hadfield Manganese Austenitic Steel: A Review Of Manufacturing Processes And Properties'', Islamic Azad University, Dezful, Iran

[21] PHAM M. K., NGUYEN D. N., HOANG A. T.; (2018) "Influence of Vanadium Content on the Microstructure and Mechanical Properties of High-Manganese Steel'', Hanoi University of Science and Technology, Vietnam

[22] ÇIKIT E.; (2015) "Kırıcı Ve Öğütücülerde Kullanılan Demir Esaslı Malzemelerin Yapı, Mekanik Özellikler Ve Aşınma Davranışlarının İncelenmesi'', İstanbul Teknik Üniversitesi, Fen Bilimleri Enstitüsü, Yüksek Lisans Tezi, İstanbul

[23] BROOK RJ.; Concie Encyclopedia of Advanced Ceramic Materials 1991, Pages 206-210

[24] Nurjaman F, Bahfie F, Widi A and Shofi A 2017 IOP Conf. Series: Journal of Physics: Conf. Series 817 012063

[25] Mazancova E, Ruziak I and Schindler I 2012 Archives of Civil and Mechanical Engineering 12 142 - 7

[26] Zhiqiang S, Di Zh, Guobin L. Evaluation of dry sliding wear behavior of siliconparticles reinforced aluminum matrix composites. J Mater Des 2005;26:454–8.

[27] Gul, F. (2010). Effect of boronizing surface treatment on the adhesive wear behavior of ferritic-pearlitic ductile iron, J. Fac. Eng. Arch. Gazi Univ., 25(2), 389-395.

[28] Abedi, H. R., Fareghi, A., Saghafian, H., and Kheirandish, S. H. (2010). Sliding wear behavior of a ferritic–pearlitic ductile cast iron with different nodule count. Wear, 268(3- 4), 622-628.

[29] Callister, W. D., and Rethwisch, D. G. (2011). Materials science and engineering (Vol. 5). NY: John Wiley and Sons.

[30] INANIR Z..; (2012) "Yüksek Çalışma Sıcaklıklarının Inconel 718 Alaşımının Yapısal Ve Mekanik Özellikleri Üzerindeki Etkilerinin İncelenmesi'', İstanbul Teknik Üniversitesi, Fen Bilimleri Enstitüsü, Yüksek Lisans Tezi, İstanbul

CURRICULUM VITAE

Kişisel Bilgiler

Adı, Soyadı : İbrahim ARSLAN

Eğitim

Derece	Eğitim Birimi	Mezuniyet Tarihi
Lisans	Kahramanmaraş Sütçü İmam Üniversitesi Makine Mühendisliği Bölümü	2019
Lise	Körfez Hereke Anadolu Lisesi	2012

İş Deneyimi

Yıl	Yer	Görev
2016-2017	Aslankaya Döküm Ve Mak. San. Tic. A.Ş.	Stajyer Mühendis
2017-2018	Universitat Politecnica de Catalunya, Barselona (İspanya)	Erasmus
2018-2019	Aslankaya Döküm Ve Mak. San. Tic. A.Ş.	Stajyer Mühendis
2019-Halen	Aslankaya Döküm Ve Mak. San. Tic. A.Ş.	Makine Mühendisi